Ocean Engineering 281 (2023) 114747

Contents lists available at ScienceDirect

Ocean Engineering

journal homepage: www.elsevier.com/locate/oceaneng

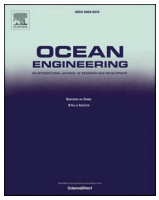

Waste heat recovery system for marine engines optimized through a preference learning rank function embedded into a Bayesian optimizer

Luis Alfonso Díaz-Secades [a,*], R. González [a], N. Rivera [a], Elena Montañés [b], José Ramón Quevedo [b]

[a] Department of Marine Science and Technology, University of Oviedo, Spain
[b] Artificial Intelligence Center, University of Oviedo, Spain

ARTICLE INFO

Handling Editor: Prof. A.I. Incecik

Keywords:
Waste heat recovery
Marine diesel engine
Desalination
Steam rankine cycle
Organic rankine cycle
Thermoelectric generators
Preference learning
Bayesian Optimization

ABSTRACT

Waste heat recovery is a proven process to improve efficiency on engines and meets current necessities of the maritime industry. Since January 1, 2023, already built vessels must meet the energy efficiency indicators known as EEXI and CII. Aiming to reduce fuel consumption and mitigate pollution emissions, a novel waste heat recovery system composed of steam Rankine cycle, organic Rankine cycle, thermoelectric harvesters and desalination is presented. High, medium and low-grade waste heat from exhaust gas, jacket water, lubricating oil and engine block radiation are targeted for recovery. Performance assessment of each subsystem when implemented on a real case study 6-cylinder medium speed marine engine is analyzed. The equivalent electricity production concept was used for the assessment of the desalination subsystem. The proposed system effectively recovers waste energy, offering economic benefits, reducing pollution and satisfying the daily demand of fresh water. Also, optimal states of the waste heat recovery are provided via Bayesian optimization, which requires an evaluation function for the system to be optimized. However, this function is not available and cannot be straightforwardly established, since the quality of waste heat recovery depends on some indicators with a trade-off among them. Hence, a preference learning procedure that exploits expert knowledge is proposed to induce a function of this kind from those indicators in order to be embedded into the Bayesian optimization procedure afterward. Applied to the case study engine, a fuel consumption reduction of 15.04% is achieved. Fuel savings lead to an improvement in energy efficiency indicators, achieving a reduction of 6.98% on the EEXI and a 13.85% on the CII.

1. Introduction

Climate change due to anthropogenic pollution is a proven fact (IPCC, 2021; Masson-Delmotte et al., 2021). According to the Fourth IMO Greenhouse Gas Study conducted by the International Maritime Organization (IMO), shipping CO2 emissions represent only 2.89% of total. Although it is a low percentage, IMO is focused on minimizing its impact and therefore it is included in its Strategic Directions (International Maritime Organization (IMO), 2022a, 2021a). Regarding greenhouse gas emissions, IMO is taking measures to reduce shipping emission levels by 40% by 2030, in relation to 2008 level. Among these, a calculation of the efficiency evaluation index for existing ships (EEXI) and annual operational carbon intensity indicator (CII), came into effect from January 1, 2023 (Czermański et al., 2022; Mallouppas and Yfantis, 2021). On top of global warming and its high impact weather effects, the world is currently affected by energy scarcity at all levels, coupled with uncertainty on peak oil production (Delannoy et al., 2021; Perifanis, 2022).

The scientific community is working towards solutions to maximize the use of available energy, as it is a faster solution than developing new technologies (Giannoutsos and Manias, 2016; Lampe et al., 2018; Ouyang et al., 2021b; Sellers, 2017). Waste heat recovery (WHR) is a proven process to improve efficiency and fits the current necessities of maritime industry. By installing WHR systems, already in use vessels do not need to exchange its propulsion and power generation systems but only make minor modifications to increase performance while saving money and cutting emissions (Butrymowicz et al., 2021; Ng et al., 2020). The steam Rankine cycle has been applied with stand-alone circuits before, but Liu et al. proposed the use of jacket water as working fluid, to avoid extra weight (Liu et al., 2020a). Organic Rankine cycles have been widely studied, especially in order to determine the best working fluid

* Corresponding author. Escuela Superior de la Marina Civil, Campus Universitario de Gijón s/n, 33203 Gijón, Asturias, Spain.
E-mail address: secadesalfonso@uniovi.es (L.A. Díaz-Secades).

https://doi.org/10.1016/j.oceaneng.2023.114747
Received 22 February 2023; Received in revised form 14 April 2023; Accepted 1 May 2023
Available online 22 May 2023

Acronyms

CAC	Charge Air Cooler
CII	Carbon Intensity Indicator
CRF	Capital Recovery Factor
EEXI	Energy Efficiency Existing ship Index
EG	Exhaust Gas
EPC	Electricity Production Cost
FO	Fuel Oil
FW	Fresh Water
GWP	Global Warming Potential
IMO	International Maritime Organization
JW	Jacket cooling Water
LMTD	Logarithmic Mean Temperature Difference
LO	Lubricating Oil
MCR	Maximum Continuous Rating
MDO	Marine Diesel Oil
ORC	Organic Rankine Cycle
RC	Rankine Cycle
SW	Sea Water
TEG	Thermoelectric Generator
WHRS	Waste Heat Recovery System
4E	Energy, Exergy, Economic and Environmental

Greek letters

η	Thermal efficiency
ψ	Exergy efficiency

(Hærvig et al., 2016; Ouyang et al., 2021a). Baldi et al. measured data from a chemical tanker and obtained an operational profile that was used to implement an optimized ORC that lead to a reduction of fuel consumption of up to 11.4% (Baldi et al., 2015). The Brayton cycle received attention as well, in particular the supercritical carbon dioxide Brayton cycle (SCBC) form due to its efficiency, size and cost (Hou et al., 2018; Ouyang et al., 2020).

The drawback of these thermodynamic cycles when used for waste heat recovery is that low-grade heat remains unused. To maximize the recovery, a combined WHR system (WHRS) capable of extracting high, medium and low-grade heat is needed (Singh and Pedersen, 2016; Zhu et al., 2020).

Already used onboard, waste heat recovery technologies like flash desalination can be integrated in a combined WHRS to recover heat contained in secondary sources, like cooling water. Furthermore, fresh water daily requirements of the vessel would be satisfied (Ouyang et al., 2019; Rose, 1983). In other cases, the nature of the heat source makes unfeasible to use systems based on circulating fluids. In a previous study, the authors determined that radiated heat from the engine block of a medium speed marine engine can account up to 10% of its shaft power (Díaz-Secades et al., 2022). In view of this, application of principles like the Seebeck effect are key to achieve maximum efficiency of marine engines.

Since the operational profile of each vessel plays a key role when obtaining its environmental indicator, Sasa et al. evaluated ship performance using an onboard measurement system (Sasa et al., 2015). Likewise, Bøckmann and Steen calculated the EEDIweather which accounts for the weather effects, in this case Beaufort 6 wind and waves (Bøckmann and Steen, 2016). In order to comply with EEXI requirements, IMO supports the use of innovative energy efficiency technologies like WHRS for generation of electricity [Category (C-1)] (International Maritime Organization (IMO), 2021b). Annual CII rating can be positively affected by using alternative fuels, performing hull cleaning, optimizing operations, speed and logistics or installing energy-saving devices and renewable energy sources (DNV, 2021; International Maritime Organization (IMO), 2021c).

In this study, a combined waste heat recovery system composed of four subsystems: steam Rankine, organic Rankine, Seebeck effect heat to electricity conversion and desalination is presented. Thermodynamic cycles and thermoelectric modules convert waste heat from different sources into electric power. Desalination satisfies freshwater daily needs onboard while achieving energy conservation and pollution reduction. In order to maximize power recovery and reduce CO2 emissions in the most economical way, a final optimization procedure taking in count these three variables is performed.

The goal of this work is to adjust the WHR system jointly optimizing exergy efficiency (ψ_{Ex}), CO_2 reduction and electricity production cost (EPC) for a specific load range. An individual optimization of one of these indicators separately from the other two does not provide optimal values for the other two. Therefore, a strategy is designed to jointly optimize those three indicators simultaneously to achieve optimal WHRS operation. The main drawback of this task is the existing trade-off between these indicators and the lack of a function able to assess the performance of WHRS from these indicators. In fact, there is no guarantee that this function may be built, since it depends on external issues that could vary dynamically in number and value. In this situation, the availability of expert knowledge makes possible to convert the problem into a preference learning task. In light of this context, experts are asked to fill different sets of WHRS' states defined in terms of the abovementioned indicators, from which experts had to decide which state among the proposed in each set is the best. This information, that is, the sets of WHRS states together with the decision of the experts (called preferences), is annotated and a rank function for assessing WHRS states was induced from it. The Support Vector Machines method is taken as the preference learner to induce the abovementioned rank function, which is able to evaluate the performance of a given WHRS state from the ψ_{Ex}, CO_2 reduction and EPC indicators. Finally, this rank function is embedded into a Bayesian Optimization procedure to obtain optimal WHRS states.

1.1. Contributions of the work

a) Analysis of a real case study vessel with data collected over the entire 2020 year.
b) Evaluation of steam Rankine and organic Rankine power cycles for the maximization of waste heat recovery, including desalination and recovery of radiated engine block heat with thermoelectrics.
c) Selection of an environmentally friendly organic Rankine working fluid that maximizes waste heat recovery.
d) The use of "equivalent electricity production" concept to quantify the contribution of the desalination system to the combined waste heat recovery system.
e) Evaluation of the influence of the proposed waste heat recovery system on the International Maritime Organization energy evaluation indices EEXI and CII.
f) Providing a rank function through a preference learning procedure for assessing the quality of WHRS states.
g) Providing a human interpretable explanation of the rank function.
h) Searching for optimal WHRS states though a Bayesian optimization taking the rank function as fitness function.

2. System configuration and working fluids

2.1. Case study vessel

In this paper, the MV Cristina Masaveu has been used as a case study

vessel. The ship, a cement carrier with a length of 133.50 m and 8291 GT, was built in 2011 and is propelled by two Wärtsilä 6L32 engines. The vessel typically operates in round trips between Spain and the UK. Characteristics of the case study engine are shown in Table 1.

The required data for the study was collected onboard during 2020, measured in 1-min intervals and previously used in a 4E analysis. The study concluded that the engine block and its auxiliaries radiate 369 kW of waste heat while the engine is running at 100% MCR (Díaz-Secades et al., 2022).

2.2. System working process

Fig. 1 displays the proposed waste heat recovery system. Since the engine has multiple grades of waste heat available, a combination of recovery systems was applied.

First, a fixed mass of jacket water enters the desalination system. This device is used to satisfy the daily needs of fresh water onboard. The remainder jacket water mass flow is used on the steam and organic Rankine cycles. The steam Rankine cycle subsystem extracts heat collected by jacket water inside the engine, and heat contained in the exhaust gas. Heat collected by lubricating oil is considered to be fully transferred into jacket water. Consequently, the RC has a preheater (engine to JW) and a main evaporator (EG to JW). Since the available heat on the exhaust gas is not enough to vaporize all the jacket water available, an organic Rankine cycle was implemented as a second waste heat recovery subsystem with JW acting as heat source. In this way, jacket water is distributed into the three abovementioned subsystems. The last subsystem on the proposal consists of thermoelectric generators, which are modules that recover low-grade waste heat and convert it into useable electric power due to the Seebeck effect. All subsystems in this proposal utilize sea water for cooling.

2.3. Mathematical model, constraints and assumptions

The mathematical model was developed by using MATLAB R2021b and CoolProp 6.4.1 database (Bell et al., 2014).

For the construction of the mathematical model, several assumptions were adopted:

1. Ambient conditions were set as per ISO 15550 (temperature 298 K, pressure 1 bar).
2. Working fluid for the organic Rankine subsystem is always stable during operation.
3. Pressure drops on pipes were considered negligible.
4. Heat loss in pipes and RC + ORC heat exchangers was considered negligible.
5. Valves installed in the system behave as adiabatic.

3. System modeling

This section introduces the step-by-step calculation process and performance analysis of the proposed waste heat recovery system.

Table 1
Engine particulars of case study engine (Wärtsilä, 2021).

Engine particulars	
Cylinder number	6
Strokes	4
Engine output at 100% MCR	3000 kW
Speed	750 rpm
Bore	320 mm
Stroke	400 mm
Compression ratio	16.0
Firing order CW	1-5-3-6-2-4
Maximum combustion pressure	192 bar

3.1. Diesel engine

The marine engine acts as heat source for the novel waste heat recovery system proposed. According to a previous work, case study engine has a thermal efficiency of 40.53% (Díaz-Secades et al., 2022). Therefore, almost 60% of the energy contained in the fuel is dissipated to the environment in the form of thermal energy. Heat sources inside the engine and included in this study are exhaust gas and jacket water. In regard to jacket water, its temperature at engine outlet does not vary under different loads. As per manufacturer instructions, water needs to enter the engine at a minimum of 323 K. In order to safeguard operation and prevent cold combustion, which will eventually result in an output power reduction, all WHR subsystems were designed so JW returns to the engine at 328 K. Heat from lubricating oil is considered to be fully transferred into the jacket water.

3.2. Desalination

A flash evaporator is already installed in the case study vessel. The device is capable of distillate up to 22 m^3 of fresh water per day. Daily needs onboard case study vessel for both industrial processes and human consumption are 12 m^3. Particulars of the system are shown in Table 2.

Waste heat recovery from jacket water residual heat and its use for desalination is a mature technology (Gude, 2019; Rose, 1983). In this occasion, it was included since it helps to maximize waste heat recovery from jacket water. By itself, desalination system does not take all the waste heat contained on JW and neither do RC and ORC subsystems alone. But if combined, a better use of the waste energy is achieved. Necessary jacket water mass flow for desalination is calculated by:

$$m_{JW\_des} = \frac{K_{jw} \cdot Daily\ capacity \cdot \rho_{sw}}{(T_{JWin} - T_{JWout})} \tag{1}$$

where K_{jw} is a constant for one stage freshwater generators [$K_{jw} = 25.6$, (Alfa Laval Copenhagen, 2006)], T_{JWin} and T_{JWout} are the temperatures of jacket water inlet and outlet of desalination system, respectively. And ρ_{sw} is the density of sea water. Once JW mass flow for desalination is known, the remaining can be used on the other subsystems.

The heat contained in the jacket water is split into the heat dedicated to desalination and the thermal energy radiated to the environment, which is calculated by Stefan Boltzmann law.

$$Q_{JWdes} = m_{JW\_des} \cdot Cp_{JW} \cdot (T_{JWin} - T_{JWout}) \tag{2}$$

$$Q_{radiated\_des} = \varepsilon \cdot \sigma \cdot T_{des_{surface}} \cdot S_{des} \tag{3}$$

$$Q_{SW\_des} = Q_{JW\_des} - Q_{radiated\_des} \tag{4}$$

where Cp_{JW} is the specific heat of jacket water (analyzed from a sample taken onboard $Cp_{JW} = 4.05$ kJ/kg·K). Parameter, ε represents surface emissivity of the desalination system, σ is the Stefan-Boltzmann constant, $T_{des_{surface}}$ is the temperature at the surface of the evaporator and S_{des} represents the outer area of the device.

Steam and organic Rankine cycles along with thermoelectric subsystem are all designed to recover energy by means of thermal to electric energy conversion. However, desalination uses waste thermal energy to produce fresh water, so no direct comparison between subsystems can be done. To overcome this issue, an equivalent thermodynamic performance has been previously described in the literature (Gude and Nirmalakhandan, 2009).

$$Q_{SW\_des\_equivalent} = Q_{SW\_des} \cdot \left(1 - \frac{T_{env}}{T_{des}}\right) \tag{5}$$

where T_{env} and T_{des} represent ambient temperature and vaporization temperature of the sea water at the chamber pressure, respectively.

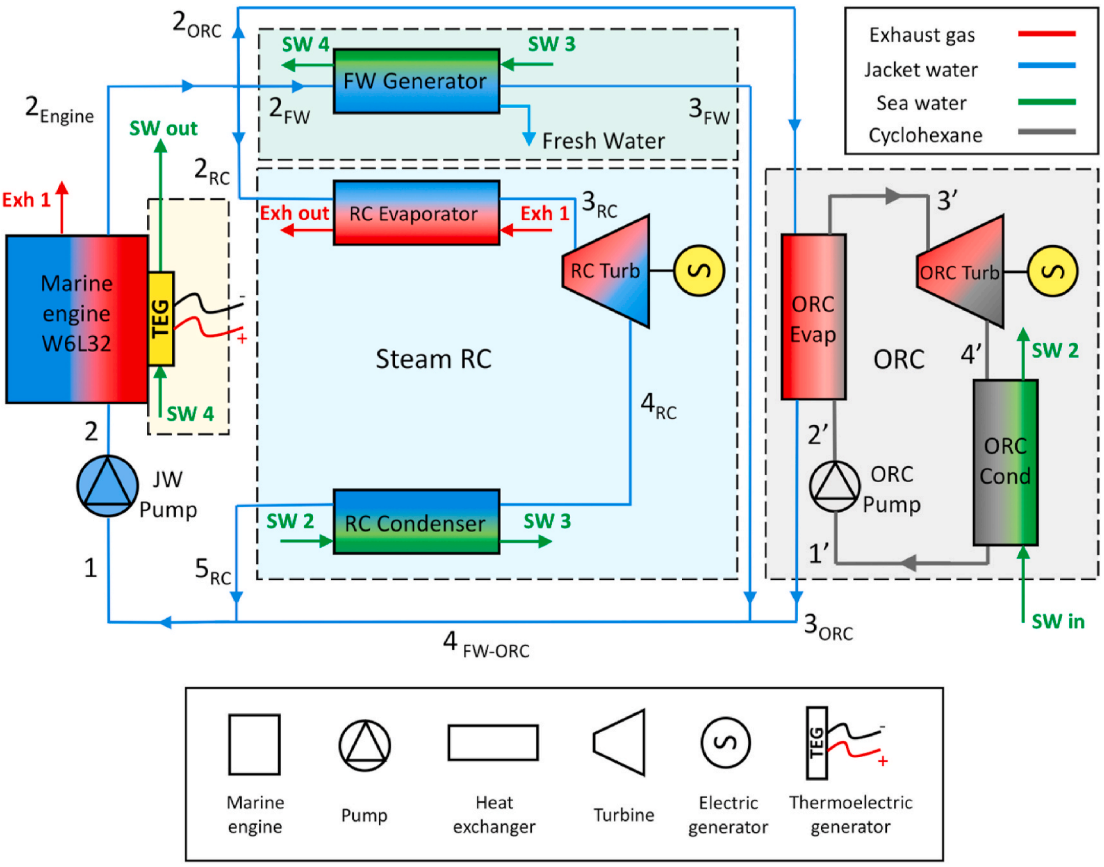

Fig. 1. Schematic diagram of the proposed WHRS.

Table 2
Particulars of desalination system installed.

Parameter	Value
Model	Facet J-100
Capacity (m^3/day)	15–22
Chamber press (bar)	0.09–0.2
Outer area (m^2)	4.8
Power consumption (kW)	10.4
Surface emissivity	0.84

3.3. Steam Rankine cycle

A steam Rankine cycle was used to recover the high-grade waste heat contained in the exhaust gas. In Table 3, specific fuel consumption and engine exhaust gas particulars under different engine load conditions are shown.

Due to acid dew point, exhaust gas temperature has to be kept over 403 K so cold corrosion is avoided. In regard to this problem, a safeguard measure was taken and outlet temperature of EG from steam Rankine evaporator was set at 413 K.

The working fluid used on the steam Rankine cycle is jacket water coming out of the engine. By doing so, extra weight is maintained as low as possible. Available waste heat on exhaust gas cannot vaporize the entire mass of jacket water, so the mass flow of JW dedicated to the Rankine cycle has to be calculated. Waste heat available on EG is obtained by:

$$Q_{exh} = m_{exh} \cdot Cp_{exh} \cdot (T_{exh_{in}} - T_{exh_{out}}) \quad (6)$$

where m_{exh} is the mass flow of exhaust gas, Cp_{exh} is the specific heat [Cp_{exh} = 1.185 kJ/kg·K, (Koshy, 2015)] and T_{exhin} and T_{exhout} are the temperatures at the inlet and outlet of RC evaporator, respectively.

Table 3
Case study engine fuel consumption, exhaust gas mass flow and temperature at different loads.

Engine load (%)	Engine power (kW)	Specific FO consumption (g/kWh)	Mass flow rate of EG (kg/s)	Temperature of EG after TC (K)
100	3000	206.0	6.24	682
95	2850	208.1	5.95	678
90	2700	210.3	5.66	675
85	2550	215.9	5.45	672
80	2400	214.5	5.08	669
75	2250	210.7	4.79	666
70	2100	206.6	4.50	657
65	1950	202.8	4.21	648
60	1800	198.7	3.92	639
55	1650	194.8	3.63	630
50	1500	185.9	3.29	622
45	1350	186.9	3.05	616
40	1200	183.9	2.76	611
35	1050	179.0	2.47	605
30	900	175.1	2.18	600

Heat absorbed by jacket water on Rankine cycle evaporator is used for three purposes: heating up to vaporization point, liquid to vapor phase change and steam superheat. All steam and organic Rankine evaporators and condensers on the proposed system work counter flow and were modeled following a three-zone methodology considering a drop of pressure on the working fluid of 0.1 bar. Fig. 2 shows the process in the RC evaporator.

Heat absorbed by jacket water is calculated by:

$$Q_{JW\_RC} = m_{JW\_RC} \cdot \left\{ Cp_{JW} \cdot \left[\left(T_{evap_{JW}} - T_{JWin} \right) + \left(RC_{Superheat} \right) \right] + \Delta h_{vap_{JW}} \right\} \quad (7)$$

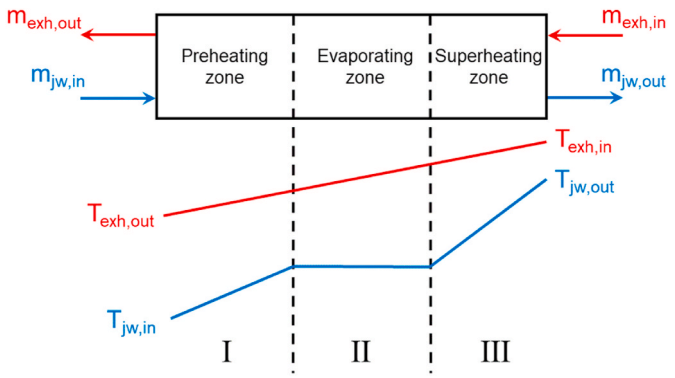

Fig. 2. Three-zone modelling of RC evaporator.

where $T_{evap_{JW}}$ is the vaporization temperature of jacket water, $RC_{superheat}$ is the superheat applied and $\Delta h_{vap_{JW}}$ is the vaporization latent heat. Mass flow of JW needed for the RC is:

$$m_{JW\_RC} = \frac{Q_{exh}}{Cp_{JW}\cdot\left[\left(T_{evap_{JW}} - T_{JWin}\right) + \left(RC_{Superheat}\right)\right] + \Delta H_{vap_{JW}}} \tag{8}$$

A common part for RC, ORC and desalination circuits is placed between the JW pump inlet and the engine outlet. Pumping work consumed by the electrical pump and its exergy destruction are calculated by:

$$W_{JW\_pump} = m_{JW}\cdot\frac{v*(P_2 - P_1)}{\varepsilon_{JW\_pump}} \tag{9}$$

$$I_{JW\_pump} = m_{JW}\cdot T_{env}\cdot(s_2 - s_1) \tag{10}$$

where v is the specific volume of jacket water at T_1 and P_1, P_1 and P_2 are the pressures at the outlet of the RC condenser and the inlet of the engine, respectively. ε_{JW_pump} is the efficiency of the JW pump and S_1 and S_2 are the entropy levels before and after the pump.

Passing through the engine, jacket water absorbs heat up to 369 K and drops 0.55 bar of pressure. Heat supplied to JW by the engine and its exergy destruction are obtained:

$$Q_{engine} = m_{JW}\cdot Cp_{JW}\cdot(T_{2c} - T_2) \tag{11}$$

$$I_{engine} = m_{JW}\cdot T_{env}\cdot(S_{2c} - S_2) \tag{12}$$

The work and exergy destruction for each subsystem can be found with their mass flow ratio.

Exergy destruction of the RC evaporation process is calculated by:

$$I_{evap\_exh} = Q_{exh}\cdot\left(1 - \frac{T_{env}}{T_{avg\_exh}}\right) \tag{13}$$

$$I_{evap_{JW\_RC}} = m_{JW\_RC}\cdot\{h_{RC3} - h_{2c} - [T_{env}\cdot(s_{RC3} - s_{2c})]\} \tag{14}$$

$$I_{RC\_evap} = I_{evap\_exh} + I_{evapJW\_RC} \tag{15}$$

where T_{avg_exh} is the LMTD average temperature of exhaust gas inside the RC evaporator, h_{2c} and h_{RC3} are the enthalpies at the inlet and outlet of the RC evaporator and so are entropies s_{RC2} and s_{RC3}. Vaporized JW enters the expander producing output work and irreversibilities:

$$W_{RC_{Turb}} = m_{JW_{RC}}\cdot(h_{RC3} - h_{RC4s})\cdot\varepsilon_{RC_{Turb}}\cdot\varepsilon_{RC_{Gen}} = m_{JW_{RC}}\cdot(h_{RC3} - h_{RC4})\cdot\varepsilon_{RC\_Gen} \tag{16}$$

$$I_{RC\_Turb} = m_{JW\_RC}\cdot T_{env}\cdot(s_{RC4} - s_{RC3}) \tag{17}$$

where h_{RC4s} and h_{RC4} are the enthalpies of the isentropic and real expansion, respectively. Entropy of JW after expansion is represented by s_{RC4}. The parameter ε_{RC_Gen} represents the efficiency of the electrical generator coupled to the turbine.

After the turbine, jacket water returns to liquid state in the steam Rankine condenser. Heat released to sea water and exergy destruction on the condenser are calculated by:

$$Q_{RC\_Cond} = m_{JW\_RC}\cdot(h_{RC4} - h_1) \tag{18}$$

$$I_{RC\_Cond\_JW} = m_{JW\_RC}\cdot\{h_{RC4} - h_1 - [T_{env}\cdot(s_{RC4} - s_1)]\} \tag{19}$$

$$I_{RC\_Cond\_SW} = m_{sw}\cdot\{h_{SW3} - h_{SW2} - [T_{env}\cdot(s_{SW3} - s_{SW2})]\} \tag{20}$$

$$I_{RC\_Cond} = I_{RC\_Cond\_JW} + I_{RC\_Cond\_SW} \tag{21}$$

Finally, net power output, exergy destruction along with thermal and exergy efficiencies of RC subsystem are obtained:

$$W_{RC\_net} = W_{RC\_Turb} - \left(W_{HT_{Pump}}\cdot\frac{m_{JW_{RC}}}{m_{JW}}\right) \tag{22}$$

$$I_{RC\_Tot} = \left(I_{HTPump}\cdot\frac{m_{JW_{RC}}}{m_{JW}}\right) + \left(I_{engine}\cdot\frac{m_{JW_{RC}}}{m_{JW}}\right) + I_{RC_{Evap}} + I_{RC\_Turb} + I_{RC\_Cond} \tag{23}$$

$$\eta_{RC} = \frac{W_{RC\_net}}{Q_{exh}} \tag{24}$$

$$\psi_{RC} = \frac{W_{RCnet}}{W_{RC\_net} + I_{RC\_Tot}} \tag{25}$$

3.4. Organic Rankine cycle

After careful comparison, R1233zd(E) was chosen as the organic Rankine working fluid due to its low GWP, safety of use and competitive performance. Once the necessary jacket water mass flows for desalination and steam Rankine subsystems are found, the remaining jacket

Table 4
Design parameters of WHRS.

Parameter	Value	Units	Reference
General			
Pumps efficiency (JW and ORC)	0.75		Ouyang et al. (2021b)
Isentropic efficiency of expanders (RC and ORC)	0.8		Liu et al. (2020b)
Efficiency of electric generators (RC and ORC)	0.96		As per electric shaft generator attached to case study engine
Pressure drop in RC and ORC evaporators and condensers	0.1	bar	Lecompte et al. (2015)
SW pressure	2.4	bar	Case study vessel
SW mass flow	42.88	m^3/h	Case study vessel
SW temperature	288.15	K	Case study vessel
Steam Rankine cycle			
JW pump pressure	3	bar	Case study engine
JW mass flow	60	m^3/h	Case study engine
RC superheat	10	K	Initial design condition
RC subcooling	2	K	Initial design condition
Organic Rankine cycle			
ORC evaporation pressure	6	bar	Initial design condition
ORC working fluid mass flow	7	m^3/h	Initial design condition
ORC superheat	4	K	Initial design condition
ORC subcooling	2	K	Initial design condition
Desalination			
Pinch point temperature in desalination system	10	K	Baldasso et al. (2020)
Initial pressure on desalination chamber (abs)	0.15	bar	Facet J-100 freshwater generator intermediate value
Thermoelectricity			
Number of TEG modules	100		According with TEG size and area of case study engine

water is diverted into the organic Rankine cycle subsystem where acts as heat source. Detailed design parameters are listed in Table 4. Pumping work on the ORC subsystem and its exergy destruction are, respectively:

$$W_{ORC\_pump} = m_{ORC} \cdot \frac{v \cdot (P_{ORC2} - P_{ORC1})}{\varepsilon_{ORC\_pump}} \tag{26}$$

$$I_{ORC\_Pump} = m_{ORC} \cdot T_{env} \cdot (s_{ORC2} - s_{ORC1}) \tag{27}$$

where v is the specific volume, P_{ORC1} and P_{ORC2} are the pressures at the outlet of the ORC condenser and the outlet of the pump. ε_{pump} is the efficiency of the ORC pump, and S_{ORC1} and S_{ORC2} are the entropies before and after. Heat supplied to the working fluid and exergy destruction on the ORC evaporator are:

$$Q_{ORC\_Evap} = m_{JW\_ORC} \cdot Cp_{JW} \cdot (T_{JW\_in} - T_{JW\_out}) \tag{28}$$

$$I_{evap\_JW\_ORC} = Q_{ORC\_Evap} \cdot \left(1 - \frac{T_{env}}{T_{avg_{ORC}}}\right) \tag{29}$$

$$I_{evap\_ORC} = m_{ORC} \cdot \{h_{ORC3} - h_{ORC2} - [T_{env} \cdot (S_{ORC3} - S_{ORC2})]\} \tag{30}$$

$$I_{ORC\_evap} = I_{evap\_JW\_ORC} + I_{evap\_ORC} \tag{31}$$

where $T_{avg_{ORC}}$ is the LMTD average temperature of JW inside ORC evaporator, h_{ORC2} and h_{ORC3} are the enthalpies at the inlet and outlet and so are entropies s_{ORC2} and s_{ORC3}, respectively. The vaporized fluid enters the ORC turbine producing output work and irreversibilities:

$$W_{ORC_{Turb}} = m_{ORC} \cdot (h_{ORC3} - h_{ORC4}) \cdot \varepsilon_{ORC_{Gen}} \tag{32}$$

$$I_{ORC\_Turb} = m_{ORC} \cdot T_{env} \cdot (s_{ORC4} - s_{ORC3}) \tag{33}$$

Where h_{ORC4} is the enthalpy of the real expansion. Entropy of R1233zd (E) after expansion is represented by s_{ORC4}. Parameter $\varepsilon_{ORC\,Gen}$ represents the efficiency of the ORC electrical generator. After expansion, vapor returns to liquid state in the condenser. Heat released to sea water and exergy destruction on the ORC condenser are calculated by:

$$Q_{ORC\_Cond} = m_{ORC} \cdot \{\{Cp_{ORC} \cdot [(T_{ORC4} - T_{condRC}) + ORC_{Subcool}]\} + \Delta h_{ORC}\} \tag{34}$$

$$I_{Cond\_ORC} = m_{ORC} \cdot \{h_{ORC1} - h_{ORC4} - [T_{env} \cdot (s_{ORC1} - s_{ORC4})]\} \tag{35}$$

$$I_{Cond\_SW} = m_{sw} \cdot \{h_{SW\_in} - h_{SW2} - [T_{env} \cdot (s_{SW\_in} - s_{SW2})]\} \tag{36}$$

$$I_{ORC\_Cond} = I_{Cond\_ORC} + I_{Cond\_SW} \tag{37}$$

Work, total exergy destruction, thermal and exergy efficiencies of the ORC are obtained:

$$W_{ORC\_net} = W_{ORC\_Turb} - W_{ORC\_Pump} \tag{38}$$

$$I_{ORC_{Tot}} = \left(I_{HTPump} \cdot \frac{m_{JW_{ORC}}}{m_{JW}}\right) + \left(I_{engine} \cdot \frac{m_{JW_{ORC}}}{m_{JW}}\right) +$$

$$+ I_{ORC_{Pump}} + I_{ORC_{Evap}} + I_{ORC\_Turb} + I_{ORC\_Cond} \tag{39}$$

$$\eta_{ORC} = \frac{W_{ORC\_net}}{Q_{ORC\_Evap}} \tag{40}$$

$$\psi_{ORC} = \frac{W_{ORCnet}}{W_{ORC\_net} + I_{ORC\_Tot}} \tag{41}$$

Thermodynamic cycles implemented on the combined waste heat recovery system can be clearly seen in the temperature–entropy diagrams shown in Fig. 3.

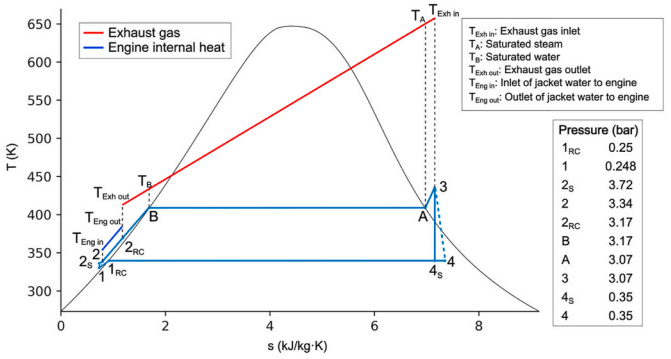

a) – T-s Diagram of the proposed Rankine cycle.

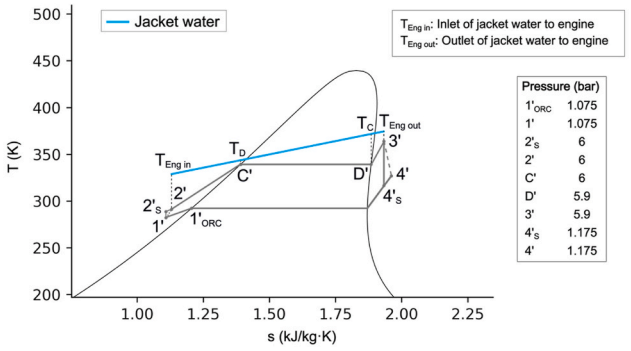

b) – T-s Diagram of the proposed ORC, working fluid R1233zd(E).

Fig. 3. T-s Diagram of the proposed RC and ORC.

3.5. Thermoelectric power conversion

After recovering the waste heat contained in exhaust gas and jacket water circuits, a residual part of low-grade waste heat remains unrecovered. To maximize energy and exergy efficiencies, this study proposes the installation of thermoelectric generators at several locations of the engine. The selection of the location was based on a previous study where it was determined that engine block, CAC and LO coolers were the best spots to recover radiated waste heat (Díaz-Secades et al., 2022).

First step in choosing a suitable TEG is the selection of materials. For the low-grade waste heat available on marine engines, Bi_2Te_3 conforms the most efficient harvester, with the advantage of being widely used for industrial applications (Champier, 2017; Nour Eddine et al., 2018; Tohidi et al., 2022).

Temperature range: After extracting the waste heat contained in exhaust gas and jacket water, the remaining heat is low-grade, with temperatures between 330 and 385 K. Under this condition, steam Rankine cycles do not work properly. An ORC could work at these temperatures (Tchanche et al., 2011) but the size and shape of the already existing engine do not favor the installation of another fluid-based circuit. On the contrary, Seebeck effect modules work at the mentioned conditions and are virtually maintenance free. In this case, commercial modules Marlow TG-12-08-1-LS made with Bi_2Te_3 were selected (Marlow Industries, 2015). Several modules can be attached to form a bigger system. For this study, a device composed of 100 TEG modules was considered. Since the environment where the engine is located is certainly harsh, a sealed version of the selected TEG was chosen. Evaluation criteria chosen for the analysis of TEG performance was exergy efficiency:

$$\psi_{TEG} = \frac{W_{TEG}}{W_{TEG} + I_{TEG}} \tag{42}$$

$$I_{TEG} = Q_{TEG} \cdot \left(1 - \frac{T_{amb}}{T_{avg_{TEG}}}\right) \tag{43}$$

$$T_{avg_{TEG}} = \frac{T_{hot} - T_{cold}}{Log\ \frac{T_{hot}}{T_{cold}}} \tag{44}$$

Manufacturer's performance curves, were used in the numerical simulation to obtain the electrical power output (Marlow Industries, 2015). The model calculates temperature gradient between hot and cold sides from input values and energy recovery from manufacturer's data.

3.6. Waste heat recovery system cooling

Sea Water is used as cooling source. The philosophy behind the sea water circuit design is to continuously extract useable energy from RC and ORC condensers, so SW heats up and enters the desalination system warmer than if it was coming in directly. By preheating the sea water, the desalination system has more energy available for vaporization. Due to the size of the proposed TEG system, its cooling does not produce a sensible rise on SW temperature and was placed last.

3.7. Evaluation of system performance

To evaluate the efficiency of the entire proposed system, electrical production along with the equivalent thermodynamic performance of the desalination system were included. Contribution of the entire waste heat recovery system was studied and net output work, exergy destruction, thermal and exergy efficiencies at different conditions analyzed. Initial parameters of the WHRS used for calculation before optimization are provided in Table 4.

3.8. Economic analysis

To assess the feasibility of the WHRS, economic parameters should be considered as well. In this study, cost, Capital Recovery Factor and Electricity Production Cost are analyzed:

$$CRF = \frac{j \cdot (1+j)^n}{(1+j)^n - 1} \tag{50}$$

$$EPC = \frac{C_{tot} \cdot (CRF + f_k)}{W_{net} \cdot t} \tag{51}$$

where j represents the interest rate and n the service life, 12% and 20 years (Emadi et al., 2020). The term t is the annual running hours (5000 running hours per year for the case study vessel). Parameter f_k is the maintenance factor, which was considered to be 8%. Although previous literature considers f_k to be 6%, an additional 2% was added due to current inflation rates (Montazerinejad et al., 2019; Nazari and Porkhial, 2020).

3.9. Environmental impact

In order to assess the environmental impact of the WHRS, CO_2 and NO_x harmful emissions reduction were calculated with the FO consumption savings obtained. For the CO_2, IPCC figures (IPCC, 2006) were used. Baseline NO_x emissions were taken from the Factory Acceptance Test record of the case study engine and account for 9.598 g/kWh.

3.10. Energy evaluation indices

Energy Efficiency Existing ship Index: Amendments to MARPOL Annex VI (International Maritime Organization - IMO, 2021), which entered into force on November 1, 2022, introduced the efficiency index EEXI for already built ships. Bulk carrier vessels of 400 GT and above must calculate attained EEXI and meet conformity with Required EEXI if 10000 DWT and above. In this work, EEXI of the case study was calculated:

$$EEXI = \frac{\left(\prod_{j=1}^{n} f_j\right) \cdot \left(\sum_{i=1}^{nME} P_{ME(i)} \cdot C_{FME(i)} \cdot SFC_{ME(i)}\right) + (P_{AE} \cdot C_{FAE} \cdot SFC_{AE}) + \left(\left(\prod_{j=1}^{n} f_j \cdot \sum_{i=1}^{nPTI} P_{PTI(i)} - \sum_{i=1}^{neff} f_{eff(i)} \cdot P_{AEeff(i)}\right) \cdot C_{FAE} \cdot SFC_{AE}\right) - \left(\sum_{i=1}^{neff} f_{eff(i)} \cdot P_{eff(i)} \cdot C_{FME} \cdot SFC_{ME}\right)}{f_i \cdot f_c \cdot f_l \cdot Capacity \cdot f_w \cdot V_{ref} \cdot f_m} \tag{52}$$

$$C_{tot} = C_{RC} + C_{ORC} + C_{Des} + C_{TEG} \tag{45}$$

where each subsystem has the cost of each piece of equipment needed, obtained as follows:

$$C = C_p \cdot F_{BM} \tag{46}$$

$$\log C_p = K_1 + K_2 \cdot \log X + K_3 \cdot (log\ X)^2 \tag{47}$$

$$F_{BM} = B_1 + B_2 \cdot F_M \cdot F_P \tag{48}$$

$$\log F_P = C_1 + C_2 \cdot \log P + C_3 (\log P)^2 \tag{49}$$

where Cp, F_{BM}, F_M, F_P and P are purchasing equipment cost, bare module factor, material factor, pressure factor and design pressure, respectively (Turton, 2018). The term X represents the capacity parameter. Cost price correction factors K_n, C_n and B_n are presented in Table 5.

Capital Recovery Factor is a ratio used to calculate the present value of an annuity and part of Electricity Production Cost formula:

where C_F represents the CO_2 conversion factor (International Maritime Organization (IMO), 2021d), *SFC* is the specific FO consumption at 75% MCR. The term *Capacity* refers to the deadweight of the vessel and V_{ref} is the speed of the vessel at 75% MCR under the draught condition corresponding to the named *Capacity*. Parameter P refers to engine power, which is usually measured at 75% MCR (International Maritime Organization (IMO), 2021e, 2021f). EEXI parameters of case study vessel are shown in Table 6.

Carbon Intensity Indicator: Along with the EEXI, an operational indicator was introduced. The CII is applicable to all cargo, RoPax, and cruise ships above 5000 GT and represents a ratio between emitted CO_2 per cargo carrying capacity and annual traveled distance. Calculation of attained CII for already in-service vessels is more straightforward than EEXI:

$$CII = \frac{M}{W} \tag{53}$$

Table 5
Cost price correction factors (Ouyang et al., 2020b).

Component	K_1	K_2	K_3	C_1	C_2	C_3	B_1	B_2	F_M	F_{BM}
Turbine	3.514	1.4398	−0.1776							3.5
Compressor	5.0335	−1.8002	0.8253							5
Pump	3.3892	0.0536	0.1538				1.89	1.35	1,5	
Condenser	4.3247	−0.303	0.1634				1.63	1.66	1	
Exchanger	4.665	0.155	0.154				0.96	1.21	1	
Evaporator	4.3247	−0.303	0.1634	0.03881	−0.11272	0.08183	1.63	1.66	1	

$$M = \sum FC \cdot C_F \tag{54}$$

$$W = Capacity \cdot Distance \tag{55}$$

where M is the mass of CO_2 emitted and W is the transport work. FC represents the total mass of diesel oil consumed in the calendar year. The term *Distance* accounts for the total of nautical miles traveled in the calendar year (International Maritime Organization (IMO), 2022b).

Attained CII value is compared with Required CII, which is obtained from the reference CII where 2019 IMO DCS data is used. From there, a CII rating is assigned (International Maritime Organization (IMO), 2021g, 2021h, 2021i).

$$CII_{Ref} = a \cdot Capacity^{-c} \tag{56}$$

$$CII_{Required} = \left(1 - \frac{Z}{100}\right) \cdot CII_{Ref} \tag{57}$$

$$CII_{Rating} = \frac{CII_{Attained}}{CII_{Required}} \tag{58}$$

where a and c are parameters obtained from IMO resolution MEPC.337 (76) and for the case study correspond with $a = 588$ and $c = 0.3885$. The term Z is a general reference for the reduction factor to be applied. This factor increases each year and for 2023 accounts for 5%, relative to 2019 (International Maritime Organization (IMO), 2021g, 2021h). In the case study vessel, currently Attained CII is 19.291 gCO_2/ton·nm, which delivers Rating E. This justifies the necessity of implementing energy recovery technologies.

3.11. The approach to the WHRS optimization

The objective is to optimize the WHRS given a load by maximizing exergy efficiency (ψ_{Ex}), reducing CO_2 emissions and minimizing electricity production cost. A black-box optimizer is the one suitable to optimize WHRS due to the impossibility of computing the derivates of the function to be optimized. Instead, this kind of optimizers just require the evaluation of the own function rather than its derivates. In this sense, Bayesian Optimization (BO) (Snoek et al., 2012) is one of the most common optimizers of this kind that has shown good performance. Then, BO solves the following task:

$$\max_x f(x) \,/\, x \in [a_1, b_2] \times \ldots \times [a_m, b_m] \tag{59}$$

where f is the function that evaluates a WHRS state (which will be defined as a rank function, in terms of the variables that computes the indicators ψ_{Ex}, CO_2 reduction and EPC), m is the number of variables involved in the computation of the indicators ψ_{Ex}, CO_2 reduction and EPC, x represents those variables and $[a_i, b_i]\ i = 1, \ldots, m$ the bounded interval of real values for each of them, since BO requires a bounded domain for the optimization space. First a function that will be included in the Bayesian optimizer is selected. The function is not straightforward to establish, and the proposal is to induce it adopting a preference learning procedure. Later on, this issue is described. Secondly, exposure of the existing tradeoff between the indicators to be optimized is done, which makes the establishment of the function to optimize difficult.

The load intervals need to be established beforehand. They were centered in values 60, 65, …, 100 with an amplitude of 5. This is necessary due to the variability in the real data collected, which is influenced by translational vessel motions such as pitching and rolling. These motions can affect the amount of load on the propeller, which is reflected in the engine, so its governor needs to be constantly adjusting the load. To account for this variability and hysteresis, the proposed intervals were used.

$$Load\ intervals \in \{[i - 2.5, i + 2.5]\} \ / \ i \in \{60, 65, 70, 75, 80, 85, 90, 95, 100\}$$

Bounds for the other seven inputs are showed in Table 7.

The need of inducing a rank function to evaluate a WHRS state through ψ_{Ex}, CO_2 reduction and EPC indicators: Investigation on whether optimizing one WHRS indicator leads to optimal values for the other two was conducted. First, one indicator is optimized to reach its optimum point for certain variable values. Then, the other two indicators are computed for these variable values. The question is whether the values of the other two indicators are also optimal. Given specific values of the load bounded in a specific interval were considered. For each of them, the indicators were optimized separately. Fig. 4 (a), (b) and (c) respectively show the values of ψ_{Ex}, CO_2 reduction and EPC when each of them is optimized. In Fig. 4 (a), ψ_{Ex} reaches its peak when optimized, but achieves lower values when either CO_2 reduction or EPC are optimized. The same occurs for CO_2 reduction, Fig. 4 (b), and for EPC in Fig. 4 (c), with the exception that the lower EPC is, the better. Thus, the conclusion is that the three indicators ψ_{Ex}, CO_2 reduction and EPC cannot reach their optimal values simultaneously at the same WHRS state.

A rank function to evaluate a WHRS system through ψ_{Ex}, CO_2 reduction and EPC indicators: The previous section highlights the challenge of optimizing all three performance indicators (ψ_{Ex}, CO_2 reduction and EPC) simultaneously. To address this issue experts can provide their knowledge, which feeds a machine learning system able to learn about which WHRS states are preferred. One advantage of this approach is that expert knowledge can be collected without the need of

Table 6
Parameters of case study vessel for EEXI calculation.

Parameter	Value
CO_2 conversion factor	3.206 gCO_2/gMDO
Propulsion power at 100% MCR	6000 kW
Deadweight	10947 t
Reference speed	15.04 kn
Required EEXI	11.2 gCO_2/ton·nm
Attained EEXI	10.6 gCO_2/ton·nm

Table 7
Bounds of input variables for the WHRS optimization, except the load.

Variable	Min bound	Max bound
JW pump	3.15	4.15
RC superheat	0	25
RC subcooling	0	10
ORC superheat	0	25
ORC subcooling	0	10
ORC pump	5.59	6.60
Desalination chamber press	0.09	0.20

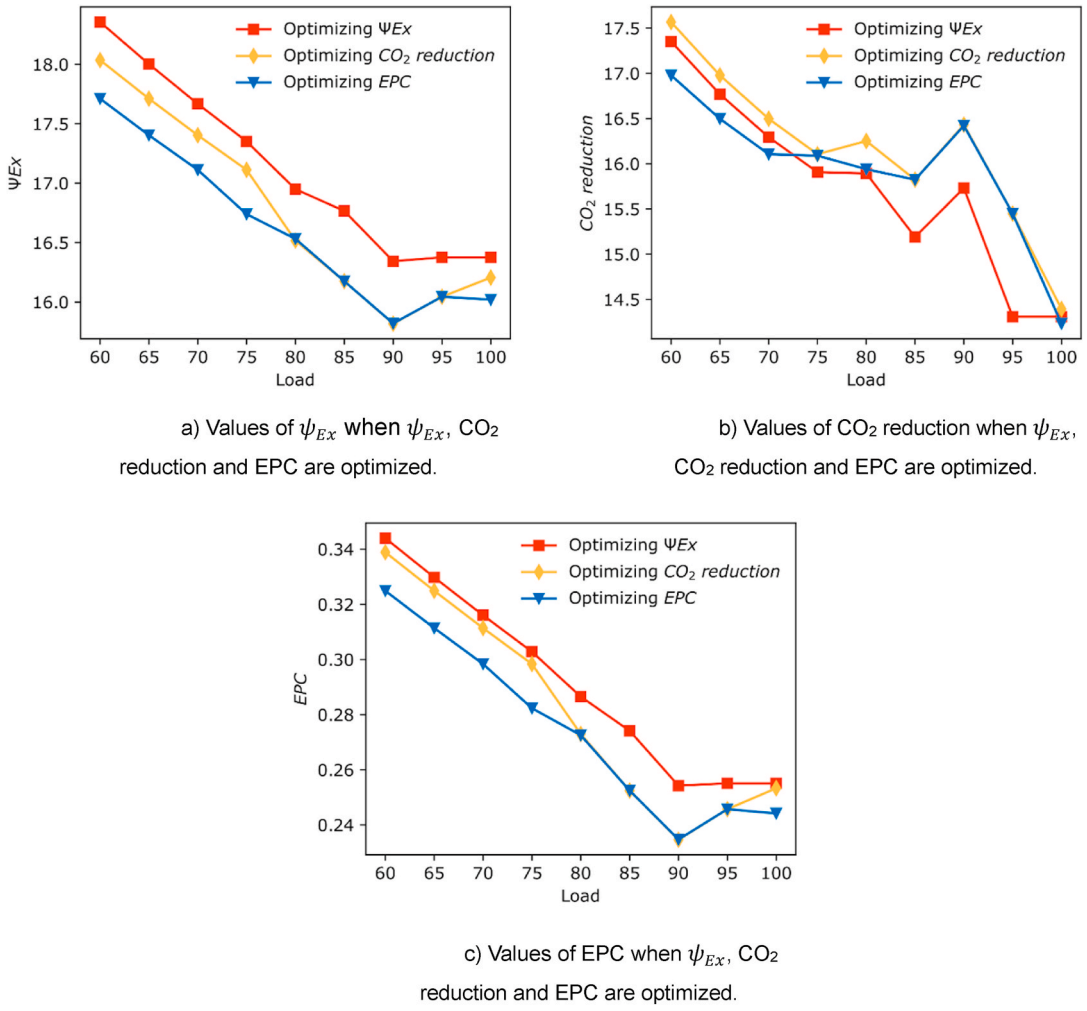

Fig. 4. Values of performance indicators when single optimizations are conducted.

expressing an explicit formula. In this sense, experts can be asked to evaluate the quality of a tern comprising the ψ_{Ex}, CO_2 reduction and EPC values. However, collecting information in this way has several drawbacks, such as batch effect and experts' bias (Bahamonde et al., 2007; Quevedo and Montanés, 2009). An alternative approach to overcome these obstacles is to ask experts for preference judgments over a set of WHRS states defined only by performance indicators. Then, these preference judgments can be used to feed a machine learning system to induce a rank function that can assess a WHRS state in terms of the variables involved in the computation of ψ_{Ex}, CO_2 reduction and EPC indicators. This rank function can be optimized through Bayesian Optimization. In this particular case, the implementation taken was Bayesian Optimization using Gaussian Processes from the library scikit-opt v0.81 (https://scikit-optimize.github.io/0.8/). Next, preference judgments generation and the induction of the rank function are detailed.

Preference judgments generation: Several values are drawn from the variables involved in computing ψ_{Ex}, CO_2 reduction and EPC indicators using a uniform distribution in the intervals that bound each variable. These values are then used to compute ψ_{Ex}, CO_2 reduction and EPC indicator values, generating several random WHRS states. The same WHRS models are considered to generate the sample to ensure coherence in the ψ_{Ex}, CO_2 reduction and EPC indicator values. From this sample of WHRS states, several preference judgment sets are built, each consisting of just a pair of WHRS states (sets of size 2) to facilitate expert decision task. The preference consists in deciding which member of each pair represents a better WHRS state in terms of ψ_{Ex}, CO_2 reduction and EPC indicator values. Some pairs of WHRS states, called doubtless pairs, are not presented to the experts, since their preference is known beforehand. These pairs are those whose values of ψ_{Ex}, CO_2 reduction and EPC in one of the sets are respectively higher, higher and lower than the other set that comprises the pair. In this case, the preference is clear due to the monotony of the ψ_{Ex}, CO_2 reduction and EPC indicators, that is, higher values of ψ_{Ex} and CO_2 reduction and lower values of EPC are preferred. Complementary pairs where ψ_{Ex}, CO_2 reduction and EPC do not agree on which situation is better are called doubtful pairs and are presented to the experts who have to decide on which member of the pair they lean towards. After this task, a sample of pairs of WHRS states with expert preferences is available to feed a machine learning system.

Inducing a rank function for WHRS state assessment with interpretable explanation through preference judgments: This section has two goals, to induce a rank function able to assess WHRS states and to give experts and users an interpretable explanation of the rank function. Inducing a linear function as rank function seems promising since ψ_{Ex} and CO_2 reduction and EPC are monotonic, meaning they are either always better as higher or always better as lower. And linear models are easier to explain than other more complex functions such as neural networks or support vector machine models with a kernel different from linear.

Let be s_1, s_2 a pair of WHRS states where s_1 is preferred to s_2, denoted by $s_1 \succ s_2$. Let also be f a function such that $s_1 \succ s_2 \leftrightarrow f(s_1) > f(s_2)$. If the function f is linear, then f satisfies $f(s_1) > f(s_2) \leftrightarrow f(s_1 - s_2) > 0 \leftrightarrow f(s_2 - s_1) < 0$. Hence,

$$s_1 \succ s_2 \leftrightarrow f(s_1 - s_2) > 0 \leftrightarrow f(s_2 - s_1) < 0 \tag{60}$$

This property makes it possible to convert the task of inducing a rank function in a preference learning context into a binary classification problem (Herbrich et al., 2000). The instances of the data that feed the classification algorithm will be represented by the values of the variables involved in the computations of ψ_{Ex}, CO_2 reduction and EPC and will be labeled by $+1$ if the experts have preferred the first member of the pair over the second and by -1 otherwise. Support Vector Machines (SVM) (Schölkopf et al., 2002; Vapnik, 1998) is a suitable classifier that can be applied for this purpose. However, evaluating the quality of the function f differs in this context from the context of a general-purpose classification problem. Under this paradigm, the c-index (Steck et al., 2007) is adopted, which computes the proportion of correctly ranked pairs.

The rank function f adopts the following expression in terms of ψ_{Ex}, CO_2 reduction and EPC indicators:

$$f(\psi_{ex}, CO_2, EPC) = a_1 \cdot \psi_{ex} + a_2 \cdot CO_2 + a_3 \cdot EPC \tag{61}$$

where a_1, a_2 and a_3 are the coefficients of the linear function learned. Despite this function is perfectly human-readable, it is not easy to interpret in the context of preference learning. In this paradigm, unlike in the classical classification of regression problem, the magnitude and signs of the coefficients are not enough to provide an interpretable explanation. However, if f is a rank function, the influence of the coefficient depends on its magnitude and if a variable (indicators ψ_{Ex}, CO_2 reduction and EPC in this case) fluctuates. In a rank function, an indicator has more influence if it varies widely and if its magnitude coefficient is high. The relative influence (RI) of each coefficient $a \in \{a_1, a_2, a_3\}$ on each indicator $v \in \{\psi_{Ex}, CO_2 \text{ reduction}, EPC\}$ can be defined as:

$$RI(a, v) = \frac{I(a, v)}{\sum_{j=1}^{3} I(a_j, v_j)} \tag{62}$$

where $I(a, v)$ is the influence of the coefficient a in the indicator v, which is computed as:

$$I(a, v) = |a| \cdot \frac{\sum_{i=1}^{n} |v_i - \bar{v}|}{n} \tag{63}$$

where n is the number of WHRS states that are compared, which in this case is the double of the number of pairs of preference generated, $\{v_i\}_{i=1}^{n}$ are the values of the indicator v for each of these WHRS states and $\bar{v}$ is the average. Then, the explanation of the rank function will be determined by the RI value of each indicator together with the sign of its correspondent coefficient. In this sense, the RI value indicate in what extent the indicator determines the rank function and the sign provides the way the value of the indicator conditions the rank value, that is, increasing the value under a positive sign and decreasing otherwise.

4. Model validation

Since the proposed waste heat recovery system is a novel arrangement, there are no relevant simulations and experiments mentioned in the literature. In order to verify accuracy and validity of the proposed system, each subsystem was validated independently.

4.1. Verification of RC

Accuracy of steam Rankine cycle subsystem was verified by comparing the results published by Liu et al. (2020a) with numerical simulation results from the model used in this study. Comparison results are shown in Fig. 5 where it is observed that simulation results have good agreement with literature data. Maximum relative errors in output power and thermal efficiency are 2.841 and 3.696%, respectively. These errors are within the allowable range, proving the reliability of the system, and can be caused by differences on the system and databases used.

4.2. Verification of ORC

For the verification of the ORC subsystem accuracy, a simulation using R1233zd(E) as working fluid was performed. Numerical simulation results of this model were compared against Ye et al. data (Ye et al., 2020). Comparison results are shown in Fig. 6 where it can be seen simulation results have good agreement with literature data. The maximum relative errors in output power and thermal efficiency are 0.876 and 3.16%, respectively. These errors are all below 5%, the allowable range, proving the reliability of the system.

4.3. Verification of desalination

Since the vessel routes in the case study are rather short and daily water consumption is lower than what the desalination system can produce, there is limited data available. Usually, with engines running at 75–85% MCR, freshwater production rate onboard is 21 m^3 per day. Table 8 shows the comparison results.

The proposed model has a relative error of 3.086–8.33% with onboard measurements. The excess of relative error can be motivated by operational wear on the system or scaling, which has not been taken into account in this study. Overall reliability of the model is verified.

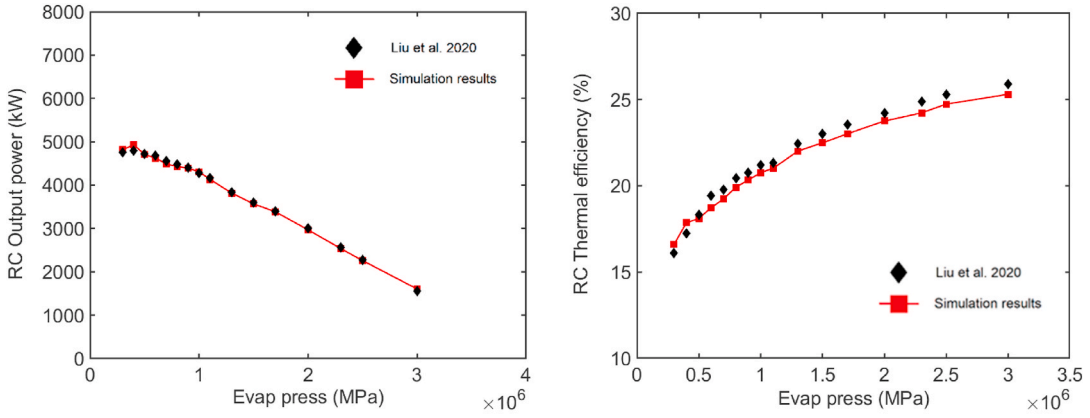

a) Rankine cycle output work. b) Rankine cycle thermal efficiency.

Fig. 5. Comparison between simulation results and previous study of JW RC.

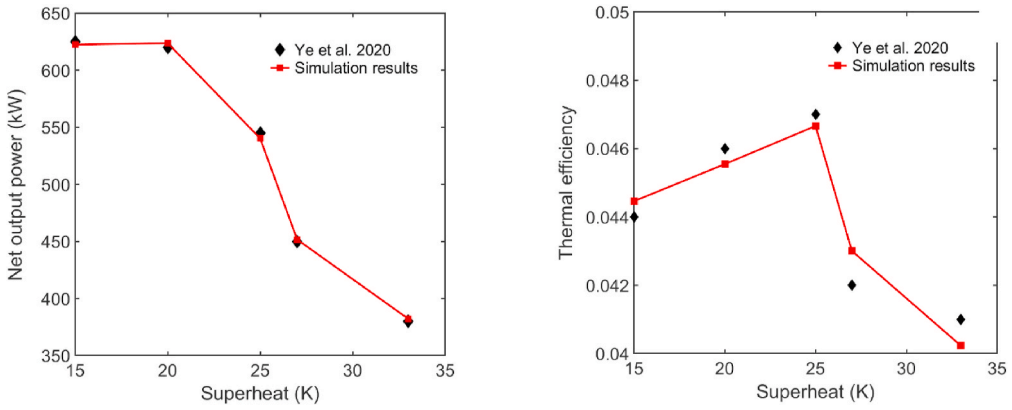

a) ORC output work. b) ORC thermal efficiency.

Fig. 6. Comparison between simulation results and previous study of ORC.

Table 8
Comparison between desalination system onboard measurements and model results.

	Water temperature	FW production (m^3/day)
Onboard measurement	369 K	21
Desalination model	369 K	21.648–22.75

5. Results and discussion

Performance parameters of each subsystem and further comparison of the efficiency of an unmodified engine against the proposed system at 100% MCR were analyzed.

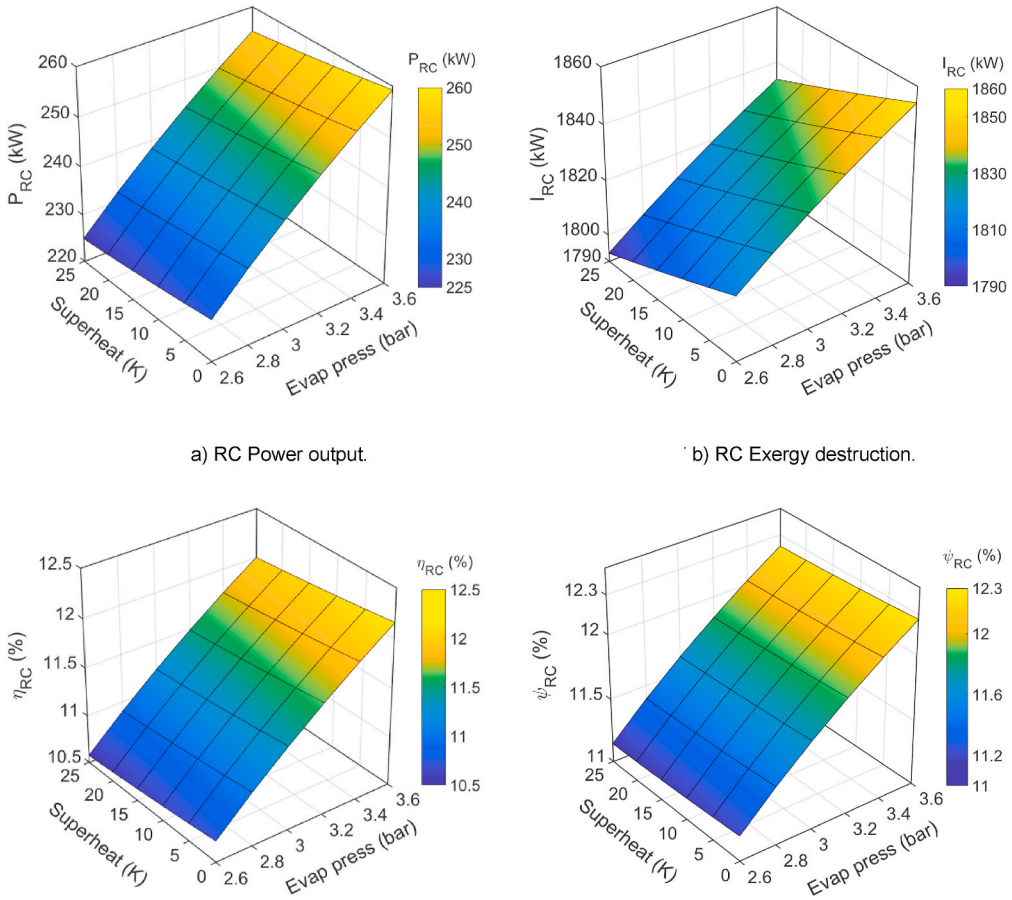

a) RC Power output. b) RC Exergy destruction.

c) RC Thermal efficiency. d) RC Exergy efficiency.

Fig. 7. Effects of evaporation pressure and superheat on RC thermodynamic performance.

5.1. RC performance

First, the effect of evaporation pressure and superheat on RC performance with a fixed subcooling of 2 K was analyzed. ORC evaporation pressure, superheat and subcooling temperature were 6 bar, 4 K and 2 K, respectively. Fig. 7 shows the effects of these parameters on output power, exergy destruction, thermal and exergy efficiencies.

It is observed that, as evaporation pressure rises, both thermal and exergy efficiencies increase. A higher evaporation pressure leads to a higher enthalpy at the outlet of the evaporator and to a larger work output. On the other hand, superheat causes a slight decrement in performance. Superheat is inversely proportional to the jacket water mass flow dedicated to the steam Rankine cycle, so higher superheat leads to a lower JW mass flow and thus a lower output work. Since the JW pump of the engine pumps the same mass flow across all conditions, superheat on the RC is mainly applied to avoid wet steam that can cause mechanical problems on the turbine, but it needs extra heat to reach higher temperatures and it is not useful for power production purposes. The highest net power output and exergy efficiency are 259.26 kW and 12.26%, respectively. These values were achieved with an evaporation pressure of 3.6 bar and 0 K of superheat. The influence of evaporation pressure on the RC is much higher than the influence of superheat, increasing exergy efficiency in 1.07% per each extra bar of pressure against a decrease of 0.02% with each extra degree of superheat. Since jacket water is used in both RC and ORC and the mass flow dedicated to the ORC depends on the amount used in the RC, the variation of RC evaporation pressure or superheat temperature affects the ORC. If any of these two RC parameters raise, ORC power output and exergy efficiency will increase slightly.

5.2. ORC performance

Once working fluid was selected, influence of evaporation pressure and superheat on organic Rankine cycle performance was analyzed. A fixed ORC subcooling of 2 K was applied. Steam Rankine cycle evaporation pressure, superheat and subcooling temperature were 3 bar, 10 K and 2 K, respectively. Fig. 8 shows the effects of these parameters on output power, exergy destruction, thermal and exergy efficiencies.

In the ORC, the effect of evaporation pressure on the system varies with the working fluid. In this particular case, using R1233zd(E), the fluctuation of the evaporation pressure also produces an increase in thermal and exergy efficiencies but slighter than in the RC. An extra bar of evaporation pressure raises thermal and exergy efficiency in 0.51 and 0.44%, respectively. The higher slope in the thermal efficiency is because of ORC heat input stays constant as long as the RC subsystem is not modified while ORC exergy destruction increases when ORC evaporation pressure is increased. In the case of superheat, higher temperatures produce a negative effect on power output and thermal efficiency but increase exergy efficiency. When a higher superheat is applied, power output and irreversibilities of the subsystem descend but the latter at a higher rate, which is enough to slightly increase exergy efficiency. As it can be observed in Fig. 3 b), R1233zd(E) is a dry fluid and does not need superheat to avoid wet steam, but can be beneficial in terms of performance. A net power output of 154.7 kW is achieved with

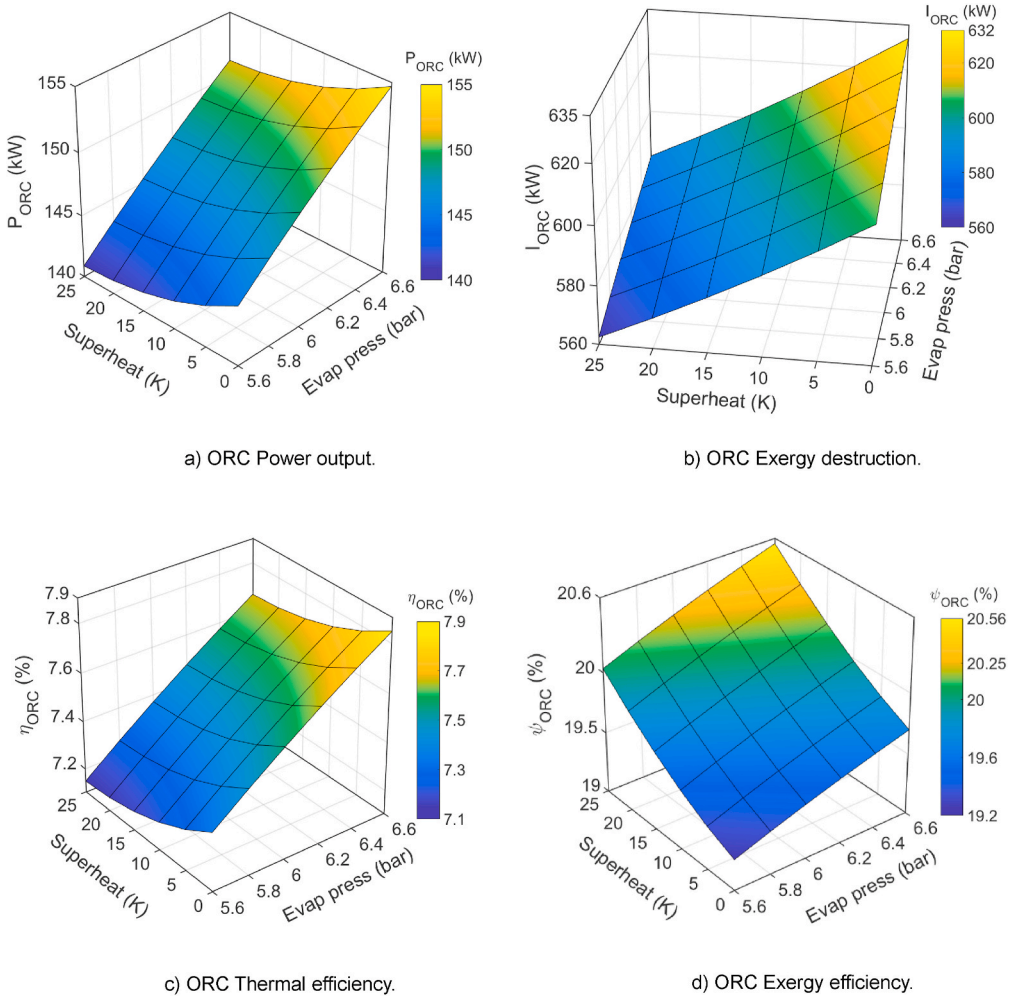

Fig. 8. Effects of evaporation pressure and superheat on ORC thermodynamic performance.

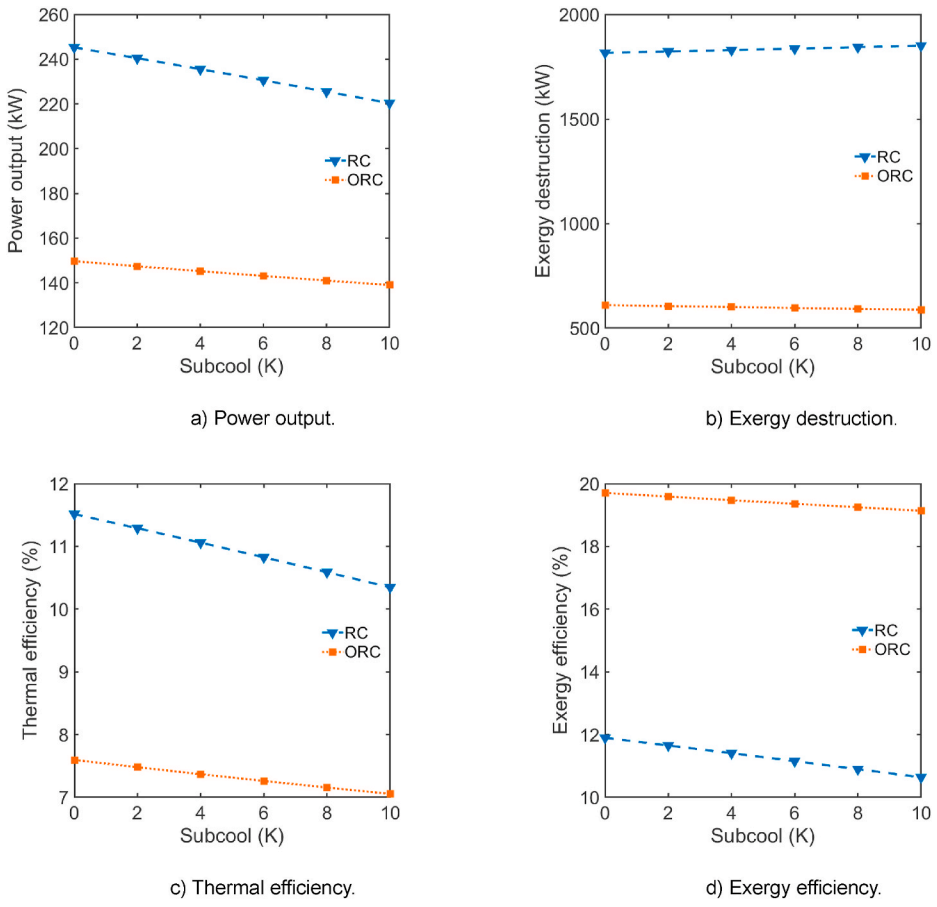

Fig. 9. Effect of RC and ORC subcooling.

an evaporation pressure of 6.6 bar and no superheat. Maximum exergy efficiency of 20.56% is reached with an evaporation pressure of 6.6 bar and 25 K of superheat. Compared to evaporation pressure, influence of superheat on the ORC is minor.

5.3. Effect of RC and ORC subcooling

Fig. 9 shows the effect of subcooling on steam and organic Rankine cycles separately. For this analysis, RC evaporation pressure and superheat were set at 3 bar and 10 K while ORC evaporation pressure was 6 bar and superheat 6 K.

In general terms, subcooling has detrimental effects on the efficiency of the plant. A higher subcooling leads to lower evaporator inlet temperatures, which reduces the power output of the cycle as more heat is needed to vaporize the working fluid. For this study, the range of subcooling applied does not vary JW or R1233zd(E) density in such a way that pumping pressure increases. In the RC, each degree of subcooling decreases thermal and exergy efficiencies in 0.117% and 0.126%, respectively. In addition, when RC subcooling increases, ORC heat input increases and this leads to a minor increment of ORC power output. When applied to the ORC, subcooling has a smaller effect. ORC thermal and exergy efficiencies decrease 0.054 and 0.056%, respectively. The subcooling on the ORC is applied to the working fluid and does not modify RC efficiency.

5.4. Desalination production

On the desalination subsystem, effects of chamber pressure and sea water temperature inlet to the recovery system were analyzed. A pinch point of 10 K was considered at the outlet of the evaporator. Fig. 10 shows their effect on FW production rate.

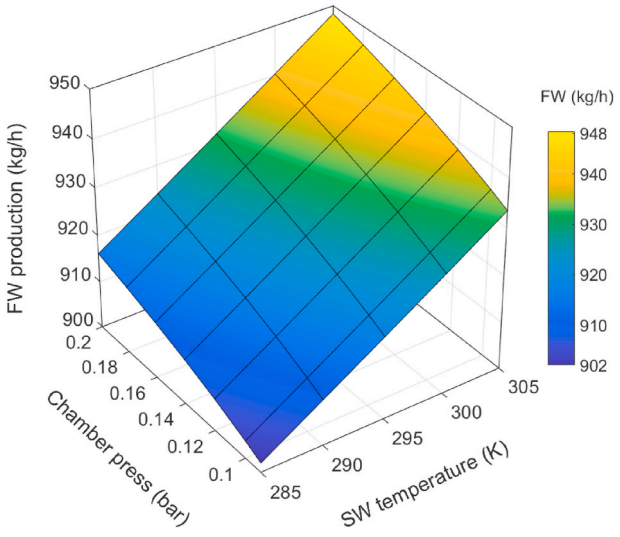

Fig. 10. Effect of chamber pressure and SW temperature on FW production.

There are two factor that primarily affect freshwater production: pressure inside the desalination chamber and sea water temperature at the inlet of the WHRS. In the case of chamber pressure, increase from 0.09 to 0.2 bar leads to a 1.55% improvement in production. Although boiling temperature of water decreases with lower pressures, latent heat is smaller with higher pressures and here leads to an increase in FW production. In the case of SW temperature, hotter SW at the inlet leads to

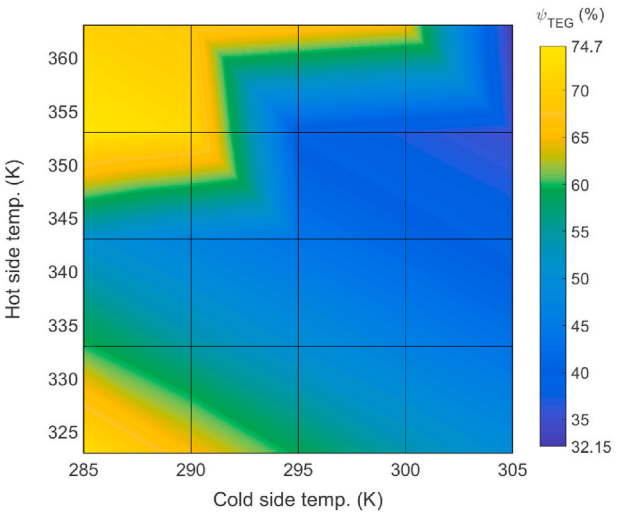

Fig. 11. Influence of temperature gradient on the exergy efficiency of the TEG.

higher FW production. This matches conclusions reached by Gude et al. (Gude and Nirmalakhandan, 2009). Since less heat is used for warming up the fluid, a greater amount of energy is available for vaporization.

5.5. Parameters of the thermoelectric conversion

Analysis of the power production achieved by thermoelectric conversion can be seen in Fig. 11. Key parameters for TEG performance are the temperatures of hot and cold sides. Since net power output produced by the TEG is much lower than RC and ORC production, exergy efficiency was chosen as evaluation criteria.

Exergy efficiency is primarily affected by the output power of the TEG and the temperature gradient between hot and cold sides. Results show that the highest exergy efficiency is achieved with the highest temperature gradients. A second area of high efficiency appears when T_{hot} is 325 K and T_{cold} is 285 K. The lower temperature gradients studied maintain output power very stably, while irreversibilities keep increasing as the temperature difference between sides increases. A higher level of irreversibilities, with a very similar output power, negatively affects TEG exergy efficiency. Once the TEG temperature gradient exceeds 333 K, output power increases enough to compensate for irreversibilities and improve exergy efficiency.

5.6. Analysis of thermodynamic performance at different engine loads

Since the major contribution to the waste heat recovery system is done by steam and organic Rankine cycles, a further comparison of these cycles was conducted. Fig. 12 reflects the amount of power recovered by RC and ORC separately along with total recovery by the entire WHRS at different engine loads. For this comparison, RC evaporation pressure was 3 bar, and superheat and subcooling were fixed to 10 and 2 K, respectively. ORC evaporation pressure, superheat and subcooling were set at 6 bar, 6 and 2 K, respectively.

Main heat sources on this proposal are exhaust gas and jacket water, complemented by engine block heat. The heat contained in the EG determines the jacket water mass flow needed for the Rankine cycle and, eventually, the power output of the subsystem. At the lowest load studied, 30%, the power extracted by the RC is as low as 52.47 kW but constantly increases up to 240.45 kW when the engine is at 100% MCR. On the other side, JW temperature at the outlet of the engine is very stable, so ORC has very little change on the power delivered. For the analysis presented in Fig. 12, lowest ORC output power was at 100% load, delivering 147.42 kW and the highest was achieved at 30% load, 155.33 kW. The difference between highest and lowest ORC power outputs is related to the heat source: since at 30% load there is less heat available in the EG, the RC needs less JW mass flow so a larger quantity is diverted to the ORC, resulting in more heat available for the ORC.

Total power extracted by the WHRS starts in 265.17 kW at 30% load, reaching 445.25 kW at 100%. If used on the case study engine with the 2020 operational profile, weighted average load would rise from 1865.12 to 2262.43 kW, which represents a 21.3% more.

5.7. Power output performance

Since best assessment of a waste heat recovery system is done by evaluating performance according to the second law of thermodynamics, an additional analysis was done. Fig. 13 shows results of exergy destruction and exergy efficiency along different engine loads.

It is observed that exergy destruction gradually increases when load is increased. When the load of the engine is low, the amount of fuel used is also lower and so does the chemical energy. This leads to lower power on the shaft and lower irreversibilities in the WHRS than at higher loads, in quantitative terms. But, if the parameter used to evaluate the recovery

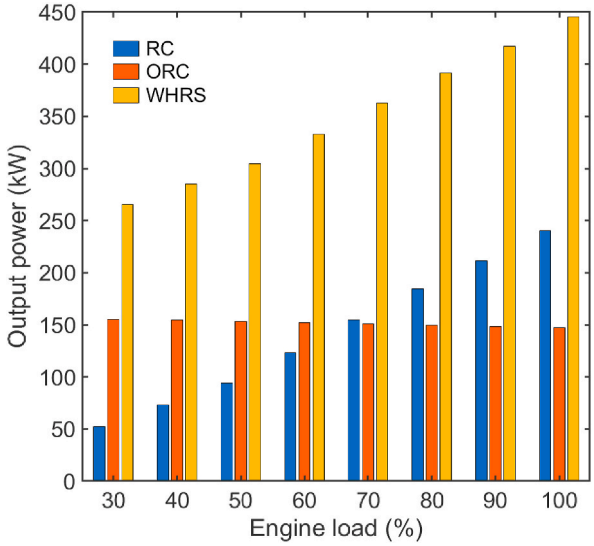

Fig. 12. Effect of steam and organic Rankine cycles on WHRS output at different engine loads.

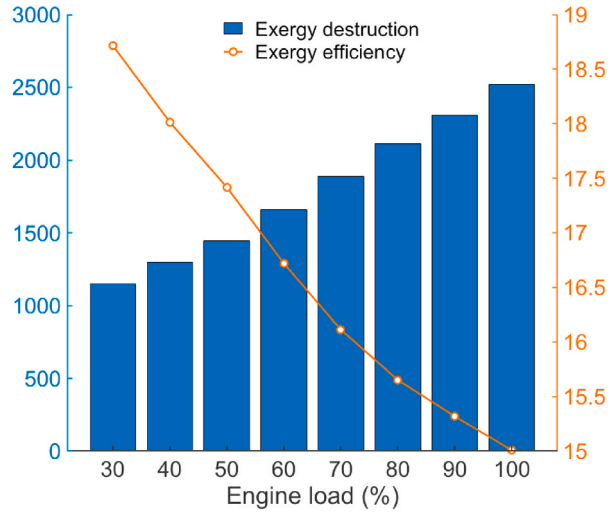

Fig. 13. Exergy destruction vs. exergy efficiency on the WHRS at different engine loads.

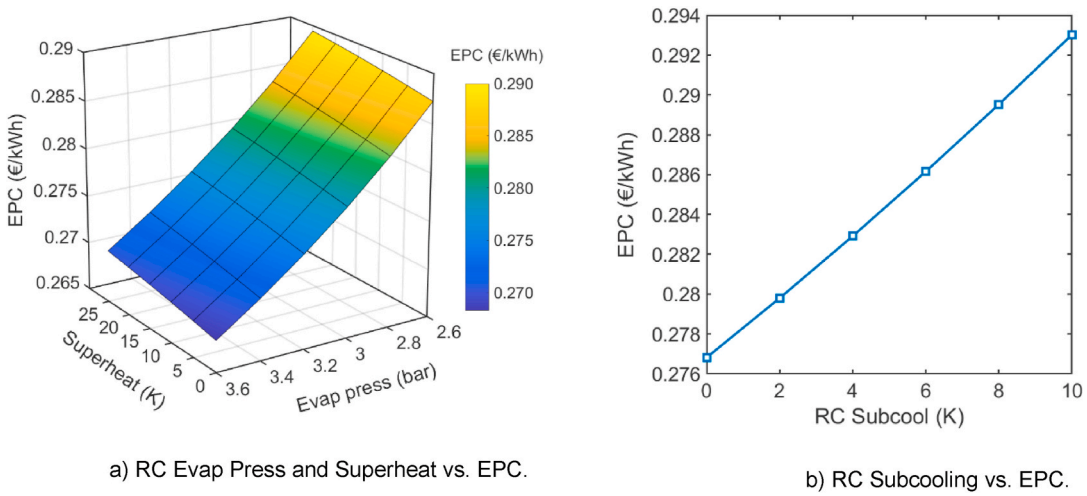

a) RC Evap Press and Superheat vs. EPC.

b) RC Subcooling vs. EPC.

Fig. 14. Influence of RC evaporation pressure, superheat and subcooling on the EPC.

system is the exergy efficiency, it can be seen that at lower loads the WHRS produces a higher amount of useful work. In this case, exergy efficiency is at its peak at 30% load, reaching 18.72% and gradually descending until the engine is at 100%, where exergy efficiency is the lowest, 15%.

5.8. Economic performance

Influence of steam Rankine cycle on economic performance when evaporation pressure, superheat and subcooling are modified was studied. Fig. 14 shows the influence of these parameters on the electricity production cost.

Fig. 14 (a) shows that EPC decreases when RC evaporation pressure increases, this is because a better RC efficiency is achieved. On the other hand, the higher the superheat, the higher the EPC due to the negative influence of superheat on RC efficiency. Fig. 14 (b) shows that RC subcooling also influences EPC, with higher subcooling temperatures resulting in higher costs. Lower temperatures on the condensate require greater amounts of heat for vaporization, which increases energy consumption and therefore the electricity production cost.

For the ORC, only evaporation pressure and superheat were analyzed. As shown in Fig. 9, the influence of subcooling on the ORC is minor. Fig. 15 shows the influence of evaporation pressure and superheat on EPC.

Similar to the RC, an increase in ORC evaporation pressure results in a decrease in EPC due to a higher ORC performance. Contrary to the RC, a higher ORC superheat has a positive effect on EPC leading to a decline in cost. Lowest EPC for the ORC is 0.236 €/kWh when both evaporation pressure and superheat are the highest levels.

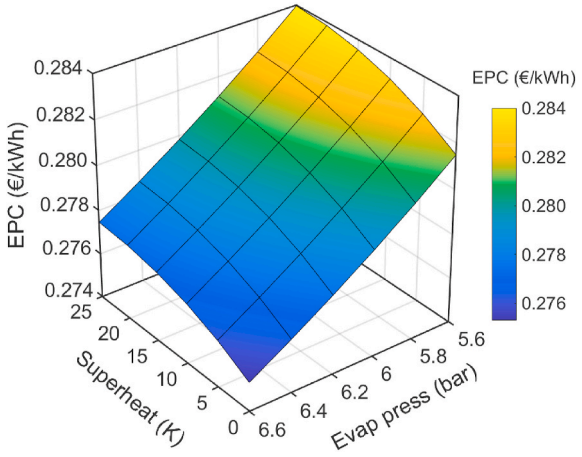

Fig. 15. Influence of evaporation pressure and superheat of ORC on EPC.

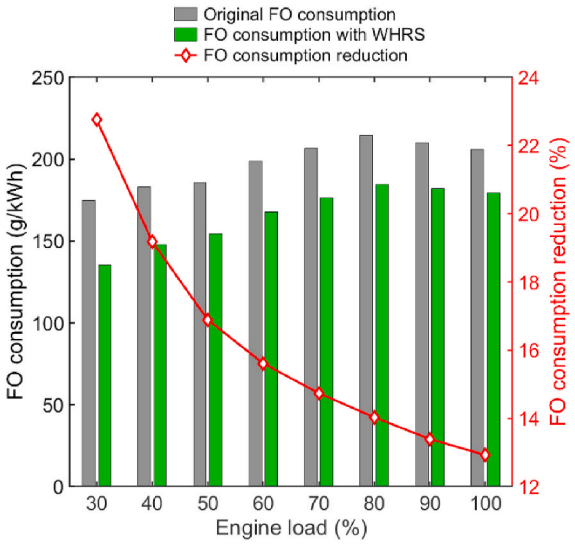

Fig. 16. FO consumption reduction at different engine loads.

5.9. Fuel savings

A clear indicator of the benefit of implementing WHR systems is the associated fuel saving. Fig. 16 shows FO consumptions measured onboard the case study vessel in contrast with FO savings and its tendency.

The largest FO consumption reduction happened at very low loads. This is because exergy efficiency at those loads is higher, as it was shown in Fig. 13. If engine load is increased, exergy efficiency of the WHRS decreases and so do FO savings. If the operational profile of the case study engine, collected during 2020 year (Díaz-Secades et al., 2022), is used to calculate a weighted average, a reduction in specific FO consumption of 29.33 g/kWh, which represents a reduction of 15.04%, is obtained.

5.10. Environmental benefit

The International Maritime Organization implemented a Sulphur cap in 2020, resulting in CO_2 and NO_x becoming the most harmful gases

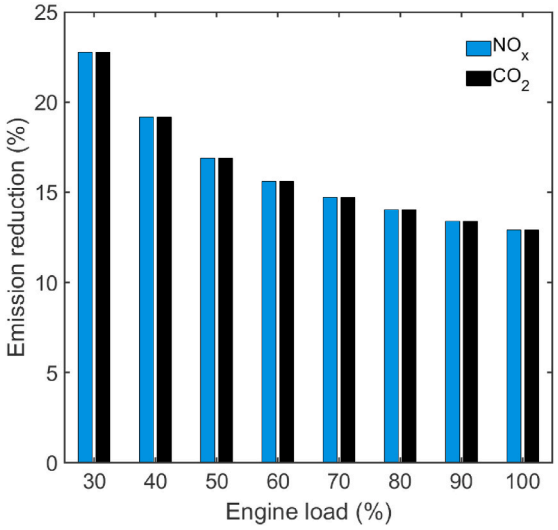

Fig. 17. CO2 and NOx emission reductions at different engine loads.

emitted by marine engines. Various lines of research are working on eliminating SO_x and mitigating the effects of CO_2 but in some cases, like ammonia, NO_x gases still persist. For this reason, the use of WHR systems is not limited to diesel machinery. Fig. 17 shows the percentage of reductions in CO_2 and NO_x emissions at the different engine loads that were studied.

The reduction in the percentage of emissions is in line with the reduction in FO consumption shown in Fig. 16, and decreases as engine load increases. Since the majority of CO_2 and NO_x emitted by marine engines are contained in the fuel used, the reduction of harmful gases is smaller at high loads. By implementing the WHRS an emission reduction of 12.9–22.7% can be achieved, depending on the engine load. If the WHRS is applied to the case study engine with the abovementioned operational profile, a reduction of 15.04% of CO_2 and 17.56% of NO_x could be achieved. This means a reduction of 2871.98 kg of CO_2 and 50.3 kg of NO_x per day.

5.11. Energy evaluation indices

Energy evaluation index for existing ships, EEXI, and carbon intensity indicator, CII, were analyzed. These indices directly reflect the impact of the WHRS on engine emissions. Table 9 shows that after the installation of the WHRS, the EEXI decreases by 0.74 gCO_2/ton·nm, which represents a reduction of 6.98%.

The original Carbon Intensity Indicator dropped a 13.85% with the application of the proposed WHRS. Table 10 shows a comparison between original CII on the case study vessel against the case when the recovery system has been applied.

These results demonstrate that system performance is improved, and emission reduction characteristics are better with the WHRS implemented.

5.12. Bayesian optimization and the rank function for assessing WHRS states

This section deals with the Bayesian optimization carried out in order to get an optimal WHRS state. First of all, the rank function to be minimized in the Bayesian optimization must be induced (see Section 5.13.1). Then, the rank function is embedded into the Bayesian optimization in order to get an optimal WHRS state (see Section 5.13.2).

Table 9
Energy efficiency index analysis.

	EEXI (gCO_2/ton·nm)
Original system	10.6
With waste heat recovery system	9.86

Table 10
Carbon intensity indicator analysis.

	CII Attained (gCO_2/ton·nm)	CII rating
Original system	19.102	E
With waste heat recovery system	16.456	C

5.12.1. Rank function induction for assessing WHRS states

A total of 50 doubtful pairs of terns were presented to three different experts to determine their preference. Experts were asked to decide which member of each pair was preferred or leave it unanswered. One expert provided answer for all 50 pairs, while the other two answered 39 and 31 pairs respectively. Therefore, a total of 120 answered pairs were available as expert preferences. In addition, other 120 doubtless pairs were prepared. Two experiments were carried out. The first one consisted of inducing the rank function from just the 120 doubtful expert answered pairs, whose expression is:

$$rf_1(\psi_{Ex}, CO_2 reduction, EPC) = 0.0613\psi_{Ex} + 0.0904 CO_2 reduction + 0.0016 EPC \quad (64)$$

The second experiment consists of inducing the rank function from both the 120 doubtful pairs answered by the experts and the 120 doubtless pairs, whose rank function was:

$$rf_2(\psi_{Ex}, CO_2 reduction, EPC) = 0.0715\psi_{Ex} + 0.0748 CO_2 reduction - 0.0023 EPC \quad (65)$$

The c-index computed through a 10-fold cross-validation was 83.33% and 84.17% for the first and second experiments, respectively.

Fig. 18 (a) and (b) show the explanation of the models in terms of Relative Influence (RI) and the sign of the coefficients. The RI of each indicator agrees with the preferences of experts in the sense that CO_2 reduction is the most relevant indicator, followed by ψ_{Ex}, but EPC clearly has the least importance. However, the sign of the coefficient of EPC is expected to be negative, since EPC is better as lower. In this sense, the performance of the second experiment, which is slightly higher with respect to the first experiment, goes accordingly with the sign of the EPC coefficient in the rank function rf_2 of the second experiment. Despite the rank functions obtained in both experiments perform similar, the inclusion of doubtless pairs conditioned the sign of the coefficients, an issue quite important for indicators whose coefficients are close to zero. Hence, doubtless pairs clearly help to guarantee the existing monotony of the indicators.

5.12.2. WHRS optimization taking rank function as target

Once a rank function that assesses a WHRS state is defined, this section includes this function as target in the BO framework stated in section 3.11. The goal is then to obtain a configuration of values for the variables involved in the computation of ψ_{Ex}, CO_2 reduction and EPC (see Table 7) that maximizes WHRS recovery.

Fig. 19 shows the indicators ψ_{Ex}, CO_2 reduction and EPC and the rank function evaluation when the WHRS is optimized for several specific load intervals of length 5 whose center is specified on the horizontal axe. As explained in section 5.8, exergy efficiency gradually decreases when the load is increased, and so does CO_2 reduction. Both parameters experience a reduction in comparison with the original system, but at a different level depending on the engine load. Conversely, as seen in equation (53), EPC gets better values at higher loads since more power is recovered.

Curiously, the best rank function value is reached at the same point on the variables independently of the load. These values are shown in Table 11.

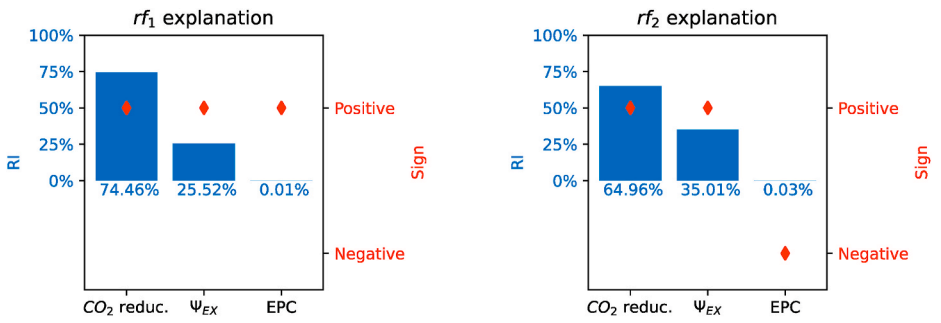

a) Relative Influence and sign of rank function's indicators learned from only the doubtful pairs.

b) Relative Influence and sign of rank function's indicators learned from both doubtful and doubtless pairs.

Fig. 18. Models explanation in terms of Relative Influence.

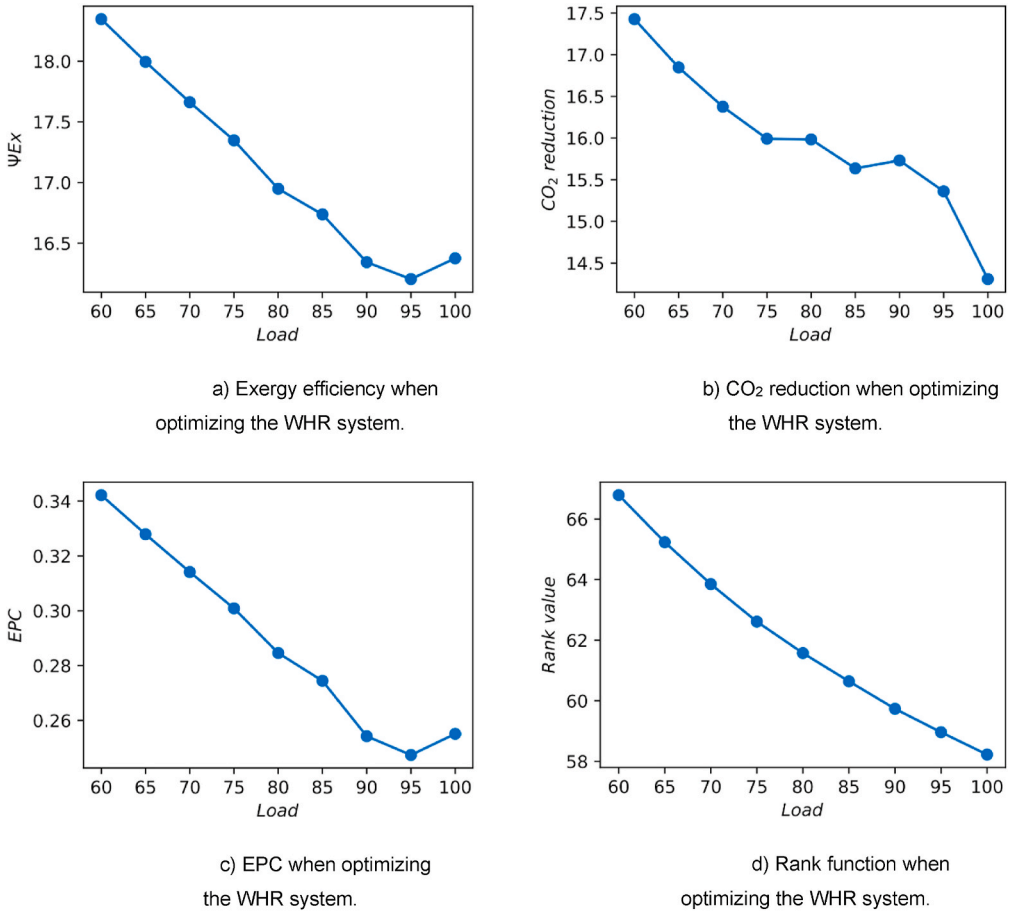

a) Exergy efficiency when optimizing the WHR system.

b) CO_2 reduction when optimizing the WHR system.

c) EPC when optimizing the WHR system.

d) Rank function when optimizing the WHR system.

Fig. 19. Values of ψ_{Ex}, CO2 reduction, EPC and rank function when optimizing the WHR system. The horizontal axis represents the center of the interval of length 5 where the load is bound.

Table 11
Optimized values for the WHRS at any engine load.

Variable	Value
JW pump	4.15
Rankine superheat	0.00
Rankine subcooling	0.00
ORC superheat	25.00
ORC subcooling	0.00
ORC pump	6.60
Desalination chamber press	0.20

6. Conclusions

This paper proposed the implementation of waste heat recovery technology to reduce fuel utilization, thus reducing the emission of harmful pollutants, in a case study vessel. A mathematical model of RC, ORC, desalination and TEG technologies was established. Evaluation of thermodynamics, economy, environment and IMO energy efficiency indicators was conducted. Main conclusions obtained from this study are as follows:

(1) With regard to the Rankine cycle, performance improvement can be achieved by selecting a high evaporation pressure and decreasing superheat as much as possible. Subcooling degree should be kept at a minimum to avoid an extra requirement of energy and thus, a lower cycle performance.
(2) The use of R1233zd(E) as ORC working fluid presents great overall performance in terms of output power, efficiency and harm to the environment. Higher ORC exergy efficiency can be attained if high evaporation pressure and high superheat are set. The degree of subcooling does not have a significant effect on ORC performance. In both RC and ORC, increasing evaporation pressure is the most effective technique to increase cycle's efficiency.
(3) Desalination via flash evaporators is a known technology for marine operators and can help to maximize JW waste heat extraction; therefore, its inclusion in a WHRS should not be underestimated. Radiated heat from the engine block and coolers is a less explored heat source that can be used with the application of the Seebeck effect.
(4) The use of innovative energy efficiency technologies for waste heat recovery and electricity generation, such as the system proposed in this work and applied to the case study, reduces specific FO consumption by 15.04%, as well as EEXI index by 6.98% and the CII indicator by 13.85%. The International Maritime Organization supports the use of energy-efficient technologies as waste heat recovery.
(5) The proposed system effectively recovers waste energy from the marine engine, offering economic benefits, reducing pollution and satisfying the daily demand of fresh water onboard.
(6) The use of preference learning to exploit expert knowledge about preferable WHRS states greatly helps to assess the WHRS system in spite of the trade-off indicators that condition its operation.
(7) Doubtless preferences clearly benefit the induction of a more accurate evaluation function of the WHRS states, particularly allowing for a more interpretable explanation of it.
(8) The embedding of the induced evaluation function into a Bayesian optimization leads to obtaining optimal states of the WHRS.

Funding

This research has been partially supported by the Spanish Ministry of Science and Innovation through the grant PID2019-110742RB-I00.

CRediT authorship contribution statement

Luis Alfonso Díaz-Secades: Conceptualization, Methodology, Writing – original draft. **R. González:** Formal analysis, Supervision. **N. Rivera:** Resources, Supervision. **Elena Montañés:** Data curation, Methodology, Software, Writing – review & editing. **José Ramón Quevedo:** Data curation, Methodology, Software, Writing – review & editing.

Declaration of competing interest

The authors declare that they have no known competing financial interests or personal relationships that could have appeared to influence the work reported in this paper.

Data availability

Data will be made available on request.

Appendix A. Supplementary data

Supplementary data to this article can be found online at https://doi.org/10.1016/j.oceaneng.2023.114747.

References

Alfa Laval Copenhagen A/S, 2006. Instruction Manual for Freshwater Generator Type D-PU-36-C100.
Bahamonde, A., Díez, J., Quevedo, J.R., Luaces, O., del Coz, J.J., 2007. How to learn consumer preferences from the analysis of sensory data by means of support vector machines (SVM). Trends Food Sci. Technol. 18, 20–28. https://doi.org/10.1016/j.tifs.2006.07.014.
Baldasso, E., Mondejar, M.E., Andreasen, J.G., Rønnenfelt, K.A.T., Nielsen, B.Ø., Haglind, F., 2020. Design of organic Rankine cycle power systems for maritime applications accounting for engine backpressure effects. Appl. Therm. Eng. 178, 115527 https://doi.org/10.1016/j.applthermaleng.2020.115527.
Baldi, F., Larsen, U., Gabrielii, C., 2015. Comparison of different procedures for the optimisation of a combined Diesel engine and organic Rankine cycle system based on ship operational profile. Ocean. Eng. 110, 85–93. https://doi.org/10.1016/j.oceaneng.2015.09.037.
Bell, I.H., Wronski, J., Quoilin, S., Lemort, V., 2014. Pure and pseudo-pure fluid thermophysical property evaluation and the open-source thermophysical property library CoolProp. Ind. Eng. Chem. Res. 53, 2498–2508. https://doi.org/10.1021/ie4033999.
Bøckmann, E., Steen, S., 2016. Calculation of EEDIweather for a general cargo vessel. Ocean. Eng. 122, 68–73. https://doi.org/10.1016/j.oceaneng.2016.06.007.
Butrymowicz, D., Gagan, J., Łukaszuk, M., Śmierciew, K., Pawluczuk, A., Zieliński, T., Kędzierski, M., 2021. Experimental validation of new approach for waste heat recovery from combustion engine for cooling and heating demands from combustion engine for maritime applications. J. Clean. Prod. 290, 125206 https://doi.org/10.1016/j.jclepro.2020.125206.
Champier, D., 2017. Thermoelectric generators: a review of applications. Energy Convers. Manag. 140, 167–181. https://doi.org/10.1016/j.enconman.2017.02.070.
Czermański, E., Oniszczuk-Jastrząbek, A., Spangenberg, E.F., Kozłowski, Ł., Adamowicz, M., Jankiewicz, J., Cirella, G.T., 2022. Implementation of the energy efficiency existing ship index: an important but costly step towards ocean protection. Mar. Pol. 145, 105259 https://doi.org/10.1016/j.marpol.2022.105259.
Delannoy, L., Longaretti, P.-Y., Murphy, D.J., Prados, E., 2021. Peak oil and the low-carbon energy transition: a net-energy perspective. Appl. Energy 304, 117843. https://doi.org/10.1016/j.apenergy.2021.117843.
Díaz-Secades, L.A., González, R., Rivera, N., 2022. Waste heat recovery from marine main medium speed engine block. Energy, exergy, economic and environmental (4E) assessment – case study. Ocean. Eng. 264, 112493 https://doi.org/10.1016/j.oceaneng.2022.112493.
DNV, 2021. CII - Carbon Intensity Indicator 1–19.
Emadi, M.A., Chitgar, N., Oyewunmi, O.A., Markides, C.N., 2020. Working-fluid selection and thermoeconomic optimisation of a combined cycle cogeneration dual-loop organic Rankine cycle (ORC) system for solid oxide fuel cell (SOFC) waste-heat recovery. Appl. Energy 261, 114384. https://doi.org/10.1016/j.apenergy.2019.114384.
Giannoutsos, S.V., Manias, S.N., 2016. Improving engine room ventilation systems: a data-driven process controller for energy-efficient, variable-speed fan operation in marine vessels. IEEE Ind. Appl. Mag. 22, 66–81. https://doi.org/10.1109/MIAS.2015.2459088.
Gude, V.G., 2019. Thermal desalination of ballast water using onboard waste heat in marine industry. Int. J. Energy Res. 43, 6026–6037. https://doi.org/10.1002/er.4647.
Gude, V.G., Nirmalakhandan, N., 2009. Desalination at low temperatures and low pressures. Desalination 244, 239–247. https://doi.org/10.1016/j.desal.2008.06.005.
Hærvig, J., Sørensen, K., Condra, T.J., 2016. Guidelines for optimal selection of working fluid for an organic Rankine cycle in relation to waste heat recovery. Energy 96, 592–602. https://doi.org/10.1016/j.energy.2015.12.098.
Herbrich, R., Graepel, T., Obermayer, K., 2000. Large margin rank boundaries for ordinal regression. Adv. Large Margin Classif. 88.
Hou, S., Cao, S., Yu, L., Zhou, Y., Wu, Y., Zhang, F., 2018. Performance optimization of combined supercritical CO2 recompression cycle and regenerative organic Rankine cycle using zeotropic mixture fluid. Energy Convers. Manag. 166, 187–200. https://doi.org/10.1016/j.enconman.2018.04.025.
Marlow Industries, 2015. Technical Data Sheet for TG12-8 Single-Stage Thermoelectric Generator 1–2.
International Maritime Organization - IMO, 2021. MEPC.328 (76) - Resolution - Amendments to the Annex of the Protocol of 1997 - 2021 Revised MARPOL Annex VI 148, pp. 148–162.
International Maritime Organization (IMO), 2021a. Fourth IMO greenhouse gas study. Int. Marit. Organ. 951–952.
International Maritime Organization (IMO), 2021b. MEPC.1-Circ, p. 896.
International Maritime Organization (IMO), 2021c. Further shipping GHG emission reduction measures adopted [WWW Document]. URL. https://www.imo.org/en/Me

diaCentre/PressBriefings/pages/MEPC76.aspx. (Accessed 11 January 2022). https://www.imo.org/en/MediaCentre/PressBriefings/pages/MEPC76.aspx.
International Maritime Organization (IMO), 2021d. Resolution MEPC 334 (76).
International Maritime Organization (IMO), 2021e. Resolution MEPC 333 (76).
International Maritime Organization (IMO), 2021f. Resolution MEPC 335 (76).
International Maritime Organization (IMO), 2021g. Resolution MEPC 338 (76).
International Maritime Organization (IMO), 2021h. Resolution MEPC 337 (76).
International Maritime Organization (IMO), 2021i. Resolution MEPC 339 (76).
International Maritime Organization (IMO), 2022a. Resolution 1.1149(32) - Revised Strategic Plan for the Organization for the Six-Year Period 2018 to 2023 9, pp. 1–29.
International Maritime Organization (IMO), 2022b. Resolution MEPC 352 (78), 1–6, 352.
IPCC, 2006. Chapter 2.3: mobile combustion. 2006 IPCC guidel. Natl. Greenh. Gas Invent. 1–78.
IPCC, 2021. Climate Change 2021: the Physical Science Basis. Contribution of Working Group I to the Sixth Assessment Report of the Intergovernmental Panel on Climate Change. Cambridge University Press, Cambridge, United Kingdom and New York, NY, USA. https://doi.org/10.1017/9781009157896.
Koshy, A.P., 2015. Exhaust gas waste heat recovery. Int. J. Innov. Res. Sci. Technol. 1, 392–400.
Lampe, J., Rüde, E., Papadopoulos, Y., Kabir, S., 2018. Model-based assessment of energy-efficiency, dependability, and cost-effectiveness of waste heat recovery systems onboard ship. Ocean. Eng. 157, 234–250. https://doi.org/10.1016/j.oceaneng.2018.03.062.
Lecompte, S., Huisseune, H., van den Broek, M., Vanslambrouck, B., De Paepe, M., 2015. Review of organic Rankine cycle (ORC) architectures for waste heat recovery. Renew. Sustain. Energy Rev. 47, 448–461. https://doi.org/10.1016/j.rser.2015.03.089.
Liu, X., Nguyen, M.Q., Chu, J., Lan, T., He, M., 2020a. A novel waste heat recovery system combing steam Rankine cycle and organic Rankine cycle for marine engine. J. Clean. Prod. 265, 121502 https://doi.org/10.1016/j.jclepro.2020.121502.
Liu, X., Nguyen, M.Q., Chu, J., Lan, T., He, M., 2020b. A novel waste heat recovery system combing steam Rankine cycle and organic Rankine cycle for marine engine. J. Clean. Prod. 265, 121502 https://doi.org/10.1016/j.jclepro.2020.121502.
Mallouppas, G., Yfantis, E.A., 2021. Decarbonization in Shipping industry: a review of research, technology development, and innovation proposals. J. Mar. Sci. Eng. 9 https://doi.org/10.3390/jmse9040415.
Masson-Delmotte, et al., 2021. IPCC, 2021: contribution of working group I to the sixth assessment report of the intergovernmental panel on climate change. Clim. Chang. 2021 Phys. Sci. Basis. 3949.
Montazerinejad, H., Ahmadi, P., Montazerinejad, Z., 2019. Advanced exergy, exergo-economic and exrgo-environmental analyses of a solar based trigeneration energy system. Appl. Therm. Eng. 152, 666–685. https://doi.org/10.1016/j.applthermaleng.2019.01.040.
Nazari, N., Porkhial, S., 2020. Multi-objective optimization and exergo-economic assessment of a solar-biomass multi-generation system based on externally-fired gas turbine, steam and organic Rankine cycle, absorption chiller and multi-effect desalination. Appl. Therm. Eng. 179, 115521 https://doi.org/10.1016/j.applthermaleng.2020.115521.
Ng, C., Tam, I.C.K., Wu, D., 2020. Thermo-economic performance of an organic rankine cycle system recovering waste heat onboard an offshore service vessel. J. Mar. Sci. Eng. 8, 351. https://doi.org/10.3390/jmse8050351.
Nour Eddine, A., Chalet, D., Faure, X., Aixala, L., Chessé, P., 2018. Optimization and characterization of a thermoelectric generator prototype for marine engine application. Energy 143, 682–695. https://doi.org/10.1016/j.energy.2017.11.018.
Ouyang, T., Su, Z., Gao, B., Pan, M., Chen, N., Huang, H., 2019. Design and modeling of marine diesel engine multistage waste heat recovery system integrated with flue-gas desulfurization. Energy Convers. Manag. 196, 1353–1368. https://doi.org/10.1016/j.enconman.2019.06.065.
Ouyang, T., Su, Z., Yang, R., Li, C., Huang, H., Wei, Q., 2020. A framework for evaluating and optimizing the cascade utilization of medium-low grade waste heat in marine dual-fuel engines. J. Clean. Prod. 276, 123289 https://doi.org/10.1016/j.jclepro.2020.123289.
Ouyang, T., Huang, G., Lu, Y., Liu, B., Hu, X., 2021a. Multi-criteria assessment and optimization of waste heat recovery for large marine diesel engines. J. Clean. Prod. 309, 127307 https://doi.org/10.1016/j.jclepro.2021.127307.
Ouyang, T., Wang, Z., Zhao, Z., Lu, J., Zhang, M., 2021b. An advanced marine engine waste heat utilization scheme: electricity-cooling cogeneration system integrated with heat storage device. Energy Convers. Manag. 235, 113955 https://doi.org/10.1016/j.enconman.2021.113955.
Perifanis, T., 2022. How US suppliers alter their extraction rates and what this means for peak oil theory. Energies 15, 821. https://doi.org/10.3390/en15030821.
Quevedo, J.R., Montanés, E., 2009. Obtaining rubric weights for assessments by more than one lecturer using a pairwise learning model. In: EDM'09 - Educational Data Mining 2009: 2nd International Conference on Educational Data Mining, pp. 289–298.
Rose, C.D., 1983. Current design and applications of marine evaporators. Mar. Technol. SNAME News 20, 348–355. https://doi.org/10.5957/mt1.1983.20.4.348.
Sasa, K., Terada, D., Shiotani, S., Wakabayashi, N., Ikebuchi, T., Chen, C., Takayama, A., Uchida, M., 2015. Evaluation of ship performance in international maritime transportation using an onboard measurement system - in case of a bulk carrier in international voyages. Ocean. Eng. 104, 294–309. https://doi.org/10.1016/j.oceaneng.2015.05.015.
Schölkopf, B., Smola, A.J., Bach, F., others, 2002. Learning with Kernels: Support Vector Machines, Regularization, Optimization, and beyond. MIT press, Cambridge, MA, US.
Sellers, C., 2017. Field operation of a 125kW ORC with ship engine jacket water. In: V, D., A, G., M, A. (Eds.), 4th International Seminar on Organic Rankine Cycle (ORC) Power Systems, ORC 2017. Elsevier Ltd, Calnetix Technologies, LLC, 16232 Shoemaker Ave., Cerritos, CA 90703, United States, pp. 495–502. https://doi.org/10.1016/j.egypro.2017.09.168.
Singh, D.V., Pedersen, E., 2016. A review of waste heat recovery technologies for maritime applications. Energy Convers. Manag. 111, 315–328. https://doi.org/10.1016/j.enconman.2015.12.073.
Snoek, J., Larochelle, H., Adams, R.P., 2012. Practical Bayesian optimization of machine learning algorithms. In: Pereira, F., Burges, C.J., Bottou, L., Weinberger, K.Q. (Eds.), Advances in Neural Information Processing Systems. Curran Associates, Inc., pp. 2951–2959
Steck, H., Krishnapuram, B., Dehing-oberije, C., Lambin, P., Raykar, V.C., 2007. On ranking in survival analysis: bounds on the concordance index. In: Platt, J., Koller, D., Singer, Y., Roweis, S. (Eds.), Advances in Neural Information Processing Systems. Curran Associates, Inc.
Tchanche, B.F., Lambrinos, G., Frangoudakis, A., Papadakis, G., 2011. Low-grade heat conversion into power using organic Rankine cycles – a review of various applications. Renew. Sustain. Energy Rev. 15, 3963–3979. https://doi.org/10.1016/j.rser.2011.07.024.
Tohidi, F., Ghazanfari Holagh, S., Chitsaz, A., 2022. Thermoelectric Generators: a comprehensive review of characteristics and applications. Appl. Therm. Eng. 201, 117793 https://doi.org/10.1016/j.applthermaleng.2021.117793.
Turton, R., 2018. Analysis, Synthesis, and Design of Chemical Processes.
Vapnik, V., 1998. Statistical Learning Theory. John Wiley, New York.
Ye, Z., Yang, J., Shi, J., Chen, J., 2020. Thermo-economic and environmental analysis of various low-GWP refrigerants in Organic Rankine cycle system. Energy 199, 117344. https://doi.org/10.1016/j.energy.2020.117344.
Zhu, S., Zhang, K., Deng, K., 2020. A review of waste heat recovery from the marine engine with highly efficient bottoming power cycles. Renew. Sustain. Energy Rev. 120, 109611 https://doi.org/10.1016/j.rser.2019.109611.
Wärtsilä 32, 2021. Product Guide. https://brandhub.wartsila.com/m/54000f75ef455f3d/original/Wartsila-32-Product-guide.pdf?utm_source=engines&utm_medium=dieselengines&utm_term=marine-power&utm_content=productguide&utm_campaign=mp-engines-and-generating-sets-gated.